Article

Cell Stem Cell

An FAK-YAP-mTOR Signaling Axis Regulates Stem Cell-Based Tissue Renewal in Mice

Graphical Abstract

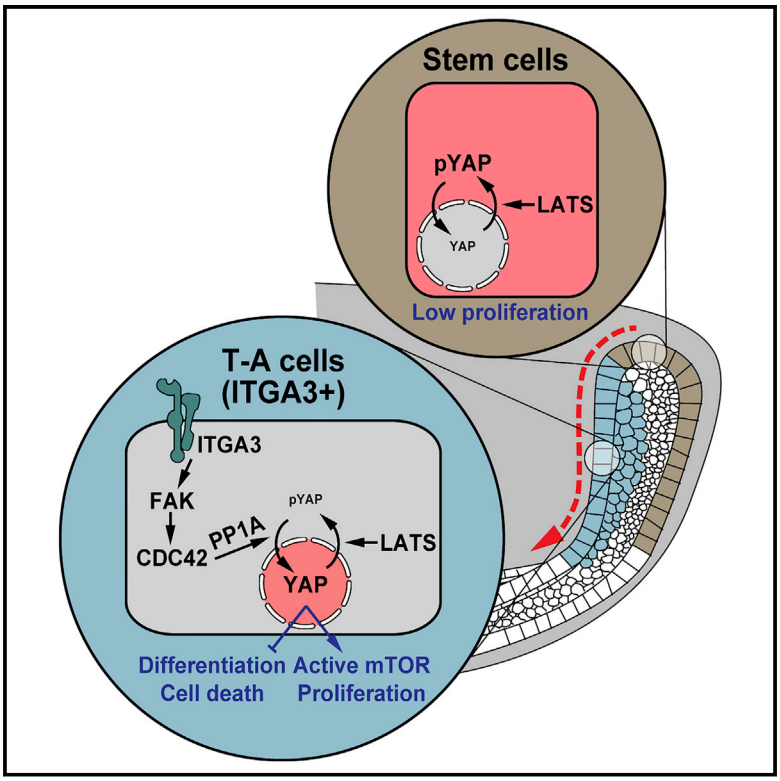

Authors

Jimmy Kuang-Hsien Hu, Wei Du, Samuel J. Shelton, Michael C. Oldham, C. Michael DiPersio, Ophir D. Klein

Correspondence

ophir.klein@ucsf.edu

In Brief

Klein and colleagues show, using the mouse incisor as a model, that the transcriptional cofactors YAP and TAZ, components of the Hippo pathway, regulate stem cell-based tissue renewal by controlling the proliferation and differentiation of transit-amplifying cells in response to integrin/FAK signaling.

Highlights

- The YAP/TAZ transcriptional cofactors are required for incisor maintenance
- YAP/TAZ prevent premature differentiation of transit-amplifying (TA) cells
- YAP/TAZ activate mTOR signaling to promote TA cell proliferation
- Integrin α3 and FAK regulate YAP nuclear localization via CDC42 and PP1A

Hu et al., 2017, Cell Stem Cell *21*, 1–16
July 6, 2017 © 2017 Elsevier Inc.
http://dx.doi.org/10.1016/j.stem.2017.03.023

CellPress

Please cite this article in press as: Hu et al., An FAK-YAP-mTOR Signaling Axis Regulates Stem Cell-Based Tissue Renewal in Mice, Cell Stem Cell (2017), http://dx.doi.org/10.1016/j.stem.2017.03.023

Cell Stem Cell
Article

CellPress

An FAK-YAP-mTOR Signaling Axis Regulates Stem Cell-Based Tissue Renewal in Mice

Jimmy Kuang-Hsien Hu,[1] Wei Du,[1,2] Samuel J. Shelton,[3,4] Michael C. Oldham,[3,4] C. Michael DiPersio,[5] and Ophir D. Klein[1,6,7,*]

[1]Department of Orofacial Sciences and Program in Craniofacial Biology, University of California, San Francisco, San Francisco, CA 94143, USA
[2]State Key Laboratory of Oral Diseases, West China Hospital of Stomatology, Sichuan University, Chengdu, Sichuan 610041, China
[3]Department of Neurological Surgery, University of California, San Francisco, San Francisco, CA 94143, USA
[4]Brain Tumor Research Center, University of California, San Francisco, San Francisco, CA 94143, USA
[5]Center for Cell Biology and Cancer Research, Albany Medical College, Albany, NY 12208, USA
[6]Department of Pediatrics and Institute for Human Genetics, University of California, San Francisco, San Francisco, CA 94143, USA
[7]Lead Contact
*Correspondence: ophir.klein@ucsf.edu
http://dx.doi.org/10.1016/j.stem.2017.03.023

SUMMARY

Tissue homeostasis requires the production of newly differentiated cells from resident adult stem cells. Central to this process is the expansion of undifferentiated intermediates known as transit-amplifying (TA) cells, but how stem cells are triggered to enter this proliferative TA state remains an important open question. Using the continuously growing mouse incisor as a model of stem cell-based tissue renewal, we found that the transcriptional cofactors YAP and TAZ are required both to maintain TA cell proliferation and to inhibit differentiation. Specifically, we identified a pathway involving activation of integrin α3 in TA cells that signals through an LATS-independent FAK/CDC42/PP1A cascade to control YAP-S397 phosphorylation and nuclear localization. This leads to *Rheb* expression and potentiates mTOR signaling to drive the proliferation of TA cells. These findings thus reveal a YAP/TAZ signaling mechanism that coordinates stem cell expansion and differentiation during organ renewal.

INTRODUCTION

As an organ ages, replacement of worn or injured tissue depends on resident somatic stem cells that have the ability to self-renew and generate differentiated cells. This stem cell-based renewal is particularly important for maintaining the homeostasis of tissues with constant cell turnover, such as the hematopoietic system, the intestinal epithelium, germ cells in the testis, and various epidermal appendages such as hair follicles and teeth (Wabik and Jones, 2015). During tissue renewal, stem cells or their proliferative descendants, known as transit-amplifying (TA) cells, divide regularly in order to meet the homeostatic demands of each tissue. The induction of stem and progenitor cell proliferation, as well as the differentiation of their progeny, must therefore be tightly regulated. Uncontrolled proliferation can lead to tissue hyperplasia (White et al., 2014; Zhou et al., 2011) and/or exhaustion of the stem cell pool (Waikel et al., 2001; Yilmaz et al., 2006), whereas the loss of stem cells' proliferative capacity disrupts normal tissue maintenance (Chen et al., 2012; Schlegelmilch et al., 2011). Thus, a central goal in stem cell biology is to understand the mechanisms that govern proliferation and differentiation of stem and TA cells in vivo.

The adult mouse incisor provides a paradigm for studying tissue renewal and regeneration. This organ continuously replaces tissues lost, as a result of abrasion from gnawing, through the activity of epithelial and mesenchymal stem cells that give rise to all adult tooth cell types, including ameloblasts and odontoblasts that produce enamel and dentin, respectively (Biehs et al., 2013; Harada et al., 1999; Juuri et al., 2012; Kaukua et al., 2014; Seidel et al., 2010). In particular, ameloblasts are derived from dental epithelial stem cells (DESCs) in the labial cervical loop (laCL), the niche region at the proximal end of the incisor (Figure 1A). Lineage tracing has shown that DESCs, marked by *Gli1*, *Bmi1*, and *Sox2*, reside in the outer enamel epithelium (OEE) and the underlying stellate reticulum (SR) of the laCL (Figure 1B) and have the capacity to both self-renew and give rise to ameloblasts and stratum intermedium cells (Biehs et al., 2013; Juuri et al., 2012; Seidel et al., 2010). The production of ameloblasts from progenitors thus resembles a conveyor belt, where the less proliferative DESCs originating from the OEE first give rise to rapidly dividing TA cells in the inner enamel epithelium (IEE) that then move distally along the length of the epithelium as they cease proliferation and undergo differentiation. Therefore, as in other tissues with constant cell turnover, the function of the incisor depends on proper regulation of TA cell proliferation and differentiation. However, what mechanisms control these processes remains an open question.

Yes-associated protein (YAP) and its homolog, transcriptional co-activator with PDZ-binding motif (TAZ), are effectors of the evolutionarily conserved Hippo signaling pathway, and they play key roles in coordinating cell proliferation and differentiation (Yu et al., 2015). For example, overexpression of activated YAP results in progenitor pool expansion, tissue hyperplasia, and altered differentiation in the skin, intestine, liver, and lung (Schlegelmilch et al., 2011; Camargo et al., 2007; Lange et al., 2015; Lu et al., 2010). Conversely, epidermal deletion of *Taz* and/or *Yap* undermines the proliferative potential of stem cells both during

Please cite this article in press as: Hu et al., An FAK-YAP-mTOR Signaling Axis Regulates Stem Cell-Based Tissue Renewal in Mice, Cell Stem Cell (2017), http://dx.doi.org/10.1016/j.stem.2017.03.023

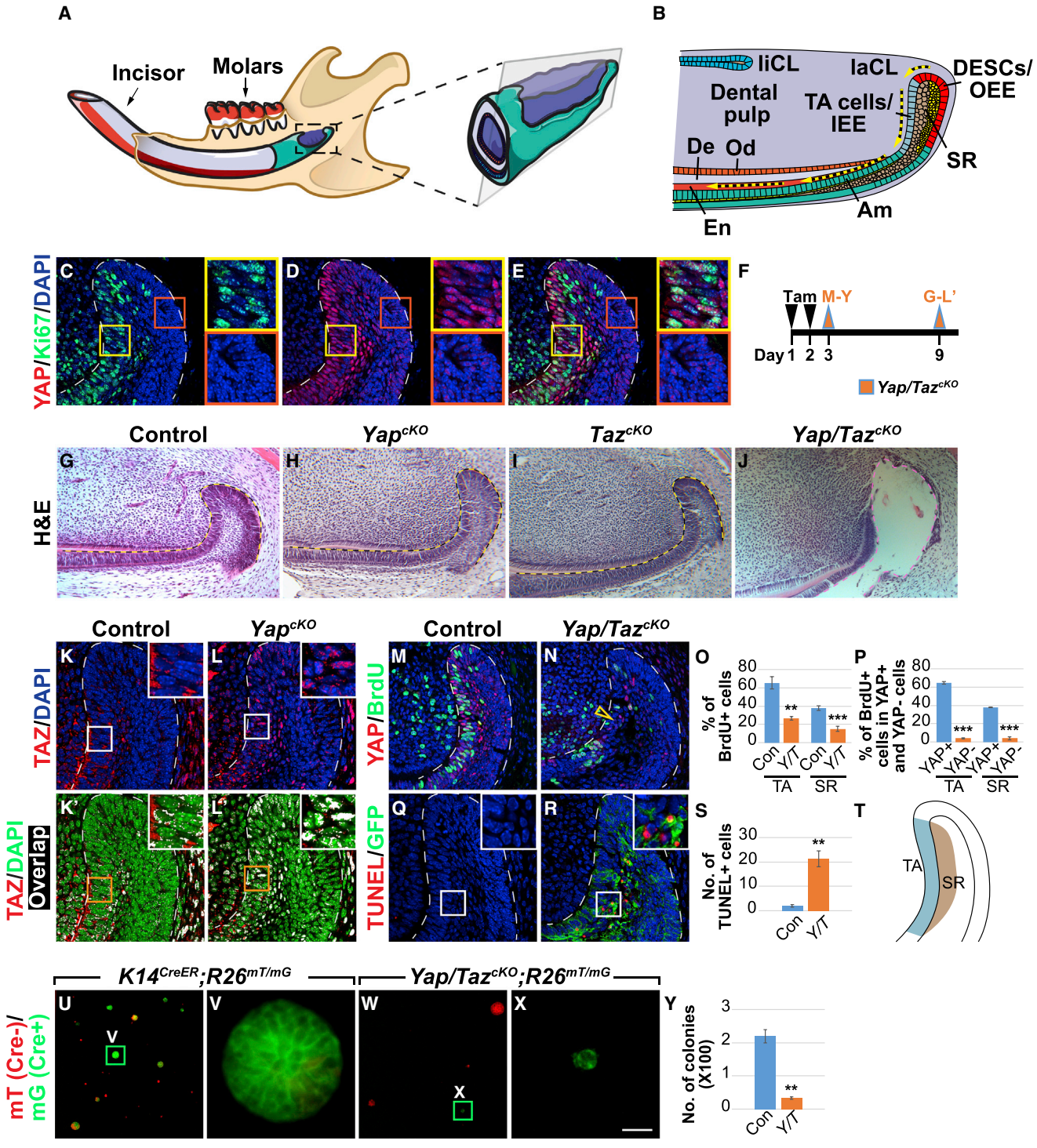

Figure 1. YAP/TAZ Are Required for the Maintenance of laCLs

(A) Schematic diagram of the mouse lower jaw.

(B) Cross section of the proximal incisor showing that, in the labial cervical loop (laCL), dental epithelial stem cells (DESCs) in the outer enamel epithelium (OEE) give rise first to transit-amplifying (TA) cells in the inner enamel epithelium (IEE) and then differentiated enamel (En)-secreting ameloblasts (Am). There are two morphologically distinct cell types in the stellate reticulum (SR), and inner SR cells underneath the TA cells also act as TA cells. De, dentin; liCL, lingual cervical loop; Od, odontoblasts.

(C–E) Immunostaining of Ki67 (C) and YAP (D) in the laCL. (E) shows a merged image. Enlarged images of TA (yellow boxes) and OEE (red boxes) regions are also displayed.

(F) Timeline depicting Cre induction (tamoxifen [Tam] injection, black arrowheads) and sample collection (orange arrowheads).

(legend continued on next page)

homeostasis and wound healing (Elbediwy et al., 2016; Schlegelmilch et al., 2011), while *Yap* is specifically required for injury repair in the intestine, mammary gland, and liver (Bai et al., 2012; Cai et al., 2010; Chen et al., 2014).

Mechanistically, the transcriptional activity of YAP/TAZ depends on their localization in the nucleus or cytoplasm, which can be regulated by diverse extracellular inputs, including cell-cell contact, mechanical stimuli, cell polarity, energy stress, and G protein-coupled receptor (GPCR) signaling (Zhao et al., 2007; Dupont et al., 2011; Szymaniak et al., 2015; Mo et al., 2015; Yu et al., 2012). These signals are in part relayed through the MAP4K/MST1/2-LATS1/2 kinase cascade, where activated phospho-LATS1/2 phosphorylate YAP/TAZ on several serine residues, including serine 127 (S127; S89 in TAZ), leading to YAP/TAZ translocation to the cytoplasm, and serine 397 (S397; S311 in TAZ), resulting in protein degradation (Zhao et al., 2010). In addition to LATS-dependent regulation, phosphorylation of YAP/TAZ can be controlled by non-LATS kinases (e.g., SRC kinase) and phosphatases (e.g., Protein Phosphatase 1A [PP1A] and PP2A) (Li et al., 2016; Schlegelmilch et al., 2011). However, as many of the studies to date focusing on YAP/TAZ regulation have been conducted in cell culture, critical questions that remain to be addressed are whether these upstream signals and regulations are physiologically relevant and how they control YAP/TAZ function to drive proper stem cell proliferation and differentiation in a tissue.

Here we report that YAP and TAZ play functionally redundant roles in the adult incisor laCL to maintain TA cell proliferation and survival, as well as to inhibit precocious differentiation. This occurs in part through the control of *Rheb* expression and subsequent effects on mTOR activation. The regulation of YAP in TA cells depends on the induction of the ITGA3-FAK-CDC42 signaling axis specifically in the TA region, which promotes interaction between PP1A and YAP and dephosphorylation on YAP-S397 in a LATS-independent manner that is distinct from the S127-guided regulation described previously. This novel regulatory pathway thus drives YAP accumulation in the TA cell nuclei, enabling the transition of stem cells into a high-proliferation TA state in order to maintain proper tissue homeostasis.

RESULTS

YAP and TAZ Are Expressed in the Nucleus and the Cytoplasm, Respectively, in Epithelial TA Cells of the Mouse Incisor

Because YAP and TAZ are important regulators of cell proliferation and differentiation, we set out to study the roles of these proteins in the regulation of adult incisor renewal. We first assessed their expression in wild-type laCLs by in situ hybridization, and we found that both *Yap* and *Taz* are abundantly expressed in the laCL (Figures S1A and S1B), with the strongest expression detected in the TA cells. As the localization of YAP and TAZ in the nucleus or cytoplasm is a key determinant of their function, we next carried out immunostaining to examine their subcellular distribution in the laCL. In accordance with the notion that nuclear YAP tends to promote proliferation, we observed high levels of nuclear YAP in the proliferating TA cells that were marked by Ki67 immunostaining and bromodeoxyuridine (BrdU) incorporation (Figures 1C–1E and 1M). This was in contrast to the low-proliferating DESC/OEE region, where we observed minimal nuclear YAP and weak cytoplasmic staining (Figures 1C–1E). A similar YAP expression pattern was also observed in the lingual CL (Figure S1C). Interestingly, the expression pattern of YAP subcellular localization in the laCL was not mirrored by TAZ, which was expressed exclusively in the cytoplasm (Figures 1K and 1K'), suggesting that YAP and TAZ are regulated differently in the laCL.

YAP/TAZ Are Required for Maintaining the laCL

To investigate the functional requirement of YAP in the laCL, we genetically deleted *Yap* in the adult dental epithelium. We crossed a *Yap* conditional allele ($Yap^{f/f}$) (Xin et al., 2011) with *Keratin 14*^{CreER} ($K14^{CreER}$) (Li et al., 2000), in which tamoxifen-inducible Cre recombinase is expressed in the incisor epithelium (Figures S1D–S1F), to generate $K14^{CreER}$;$Yap^{f/f}$ conditional knockout (cKO) mutants (Yap^{cKO}). We first examined the general architecture of the laCL by H&E staining 1 week after injection of 8-week-old mice with tamoxifen (Figure 1F). To our surprise, most Yap^{cKO} mutant laCLs were morphologically indistinguishable from the Cre-negative controls (n = 9/12) (Figures 1G and 1H), although in a minority of samples (n = 3/12) the laCLs were disorganized and exhibited small holes in the tissue (Figures S1K and S1L). We therefore considered the possibility that loss of YAP could be compensated for by TAZ, and this was supported by increased nuclear TAZ in Yap^{cKO} laCLs (Figures 1L and 1L'). As TAZ single deletion (Taz^{cKO}) had no effect on the laCL (Figure 1I), we generated Yap/Taz^{cKO} double mutants. Deletion of both *Yap* and *Taz* caused cells in the TA and SR regions to detach from one another by 4 days after Cre induction (Figures S1M and S1N), and by 7 days after Cre induction there was a remarkable tissue loss in the SR and TA regions (n = 12/12) (Figures S1O and S1P). In the most severe cases, the entire laCL was lost and a large hole developed (Figure 1J).

(G–J) H&E staining of control (G), Yap^{cKO} (H), Taz^{cKO} (I), and Yap/Taz^{cKO} (J) laCLs. Pink dashed line outlines the tissue loss in (J).

(K–L') TAZ immunostaining in control (K) and Yap^{cKO} (L) laCLs. Overlapping TAZ and DAPI staining in control (K') and Yap^{cKO} (L') laCLs is shown in white. Insets are enlargements of the TA region.

(M–P) BrdU labeling in control (M) and Yap/Taz^{cKO} (N) laCLs. Open yellow arrowhead in (N) marks reduced proliferation. Quantification was performed by calculating the percentage of BrdU-positive (+) cells per section in control and Yap/Taz^{cKO} laCLs (O) and by comparing the percentage of BrdU+ cells between YAP+ and YAP− cells in mutant laCLs (P).

(Q–S) TUNEL staining in control (Q) and Yap/Taz^{cKO} (R) laCLs shows increased cell death upon *Yap/Taz* deletion (S). GFP marks Cre active cells.

(T) Schematic diagram of the TA and SR regions used for quantification.

(U–Y) Colony formation assays in 3D matrigel. (V) and (X) are enlarged images of Cre active cells in (U) and (W). The average number of colonies (excluding single cells) per well is quantified (Y).

Dashed lines outline laCLs. Representative images and quantitative data are shown. All quantitative data are presented as mean ± SD (**$p < 0.01$ and ***$p < 0.001$). Scale bar (shown in X) represents 50 μm in (C)–(E), (K)–(N), (Q), and (R); 90 μm in (G)–(J); 240 μm in (U) and (W); and 15 μm in (V) and (X). See also Figure S1.

A similar phenotype was also observed in the lingual CL (Figure S1S and S1T), suggesting a conserved YAP/TAZ function in different populations of DESCs. The loss of tissue was confirmed by computed microtomography (μCT), which enables visualization of tissues without the potential for causing histological artifacts (Figures S1Q and S1R). Because *Yap/Taz*^{cKO} animals gradually ceased eating and became moribund 7–10 days after Cre initiation, likely due to the requirement for YAP/TAZ function in other epithelial organs, we were unable to assess the long-term consequences on mineral deposition in the distal incisor.

The dramatic loss of the laCL in *Yap/Taz*^{cKO} could be attributed to decreased proliferation, increased cell death, or both. We first measured the percentage of proliferating cells by BrdU labeling 2 days after Cre induction (Figure 1F), a time point prior to the laCL destruction. We took advantage of the mosaic nature of tamoxifen-induced Cre recombination to compare BrdU labeling in cells with and without YAP/TAZ deletion within the same laCL. While there was a significant reduction of proliferation in YAP-negative TA and SR cells, BrdU signals were still present in cells with intact YAP expression (Figures 1M–1P and 1T). We next marked apoptotic cells using terminal deoxynucleotidyl transferase dUTP nick end labeling (TUNEL). We utilized the Cre-responsive reporter allele *R26*$^{mT/mG}$ (Muzumdar et al., 2007) to identify cells that underwent Cre recombination and were permanently labeled with membrane GFP (mG) (Figures S1D–S1J'); cells lacking Cre activity continued to express membrane tdTomato (mT). Using this strategy, we noted an increase in apoptosis among *Yap/Taz*^{cKO} cells, primarily in SR and distal TA cells; apoptosis also occurred in the OEE after the loss of TA/SR cells at a later time point (Figures 1Q–1S and S1U–S1X). Lastly, we tested the role of YAP/TAZ in laCL cell expansion using in vitro colony formation assays. Dissociated cells from control *K14*^{CreER};*R26*$^{mT/mG}$ laCLs routinely formed spheroids in 3D culture, whereas GFP-positive *Yap/Taz*^{cKO};*R26*$^{mT/mG}$ mutant cells remained as single cells (Figures 1U–1Y). In contrast, *Yap/Taz*^{cKO};*R26*$^{mT/mG}$ cells that escaped Cre activation (tdTomato-positive) maintained their ability to form colonies. Together, these results demonstrate an absolute requirement for YAP/TAZ in sustaining cell proliferation and survival in the adult incisor laCL.

YAP/TAZ Prevent Precocious Differentiation in the Mouse Incisor Epithelium

As YAP/TAZ are transcriptional cofactors, we next performed gene expression profiling using RNA from control and *Yap/Taz*^{cKO} laCLs 2 days after Cre induction, allowing us to detect early changes that occurred prior to tissue destruction. Among targets that were upregulated, we found several genes that mark differentiated ameloblasts, such as *Amelogenin* and *Ameloblastin* (Figure 2A). Increased expression of these genes was confirmed by qPCR analysis, immunoblotting, and in situ hybridization (Figures 2B, 2C, and S1Y–S1AB). Finally, we performed Amelogenin and Ameloblastin immunostaining, and we observed that, while these ameloblast markers were not expressed in control laCLs, they were readily detected in the *Yap/Taz*^{cKO} SR cells (Figures 2D–2G), indicating that, in the absence of YAP/TAZ, some laCL cells undergo precocious differentiation.

YAP/TAZ Activate mTOR Signaling by Controlling Rheb Expression

Our gene expression analysis identified a set of genes that were downregulated, and gene set enrichment analysis (GSEA) revealed that the mammalian target of the rapamycin (mTOR) signaling pathway was one of the top modules affected (Table S1). In particular, expression of *Rheb* (Ras homolog enriched in brain), which encodes an activator of the mTOR Complex 1 (mTORC1), was reduced in the absence of YAP/TAZ (Figures 2A, 2B, and 3K). Furthermore, while immunostaining revealed that RHEB was expressed robustly throughout the entire TA and SR regions of control laCLs, its expression in *Yap/Taz*^{cKO};*R26*$^{mT/mG}$ was downregulated in TA and SR cells that had undergone Cre-mediated recombination, as visualized by the presence of membrane GFP (Figures 3A, 3C–3E', 3I, S2A, and S2B). These results thus suggest that mTOR signaling is compromised in *Yap/Taz*^{cKO}. We tested this hypothesis by examining the expression of phospho-P70-S6 kinase (pS6K1) and phospho-translation initiation factor 4E-binding protein (p4EBP), two readouts of active mTOR signaling (Hay and Sonenberg, 2004). In line with RHEB expression, robust staining of pS6K1 and p4EBP was detected uniformly in control TA and underlying SR cells (Figures 3F, 3F', S2E, and S2E'), while their expression was significantly decreased in *Yap/Taz*^{cKO};*R26*$^{mT/mG}$ laCLs (Figures 3G–3H', 3J, and S2C–S2J). These results were confirmed by immunoblotting (Figure 3L).

Because mTOR signaling functions as a central regulator of cell proliferation and survival (Laplante and Sabatini, 2009), we reasoned that the decreased mTOR activity in *Yap/Taz*^{cKO} could explain some of the phenotypes we observed earlier, and thus that perturbation of the mTOR pathway may partially phenocopy *Yap/Taz*^{cKO}. We first took an explant approach, in which dissected wild-type proximal incisors were cultured (Figure 3M) in the presence or absence of the mTORC1 inhibitor Rapamycin. In control samples, cells continued to proliferate, while Rapamycin-treated incisors had reduced proliferation (Figures 3N–3P). To confirm the tissue-autonomous role of mTOR signaling in laCLs, we next perturbed mTOR signaling by using *K14*^{CreER} to conditionally delete *Regulatory-associated protein of mTOR* (*Rptor*), which encodes a critical regulator of mTORC1 (Hara et al., 2002). The resultant *Rptor*^{cKO} mutants displayed a reduction in BrdU-labeled cells 18 hr after Cre induction (Figures 3B, 3Q–3S, and S2N). The importance of *Rptor* for progenitor pool expansion became even more obvious in longer-chased *Rptor*^{cKO} samples, as there was a near-complete loss of GFP-positive Cre-recombined mutant TA cells and ameloblasts, which were replaced by proliferative GFP-negative wild-type cells (Figures S2K–S2M'). Together, these results demonstrated that YAP/TAZ-mediated mTOR activation is critical for expanding the progenitor pool in laCLs.

ITGA3 and FAK Signaling Promotes Nuclear YAP Localization in laCLs

Given the critical roles that YAP/TAZ play in laCL maintenance, we set out to study the underlying mechanism that controls YAP nuclear localization in TA cells. We focused on YAP because our results above indicated that YAP is the primary regulator of TA proliferation and differentiation, with TAZ serving as a redundant alternate in the absence of YAP. To that end, we

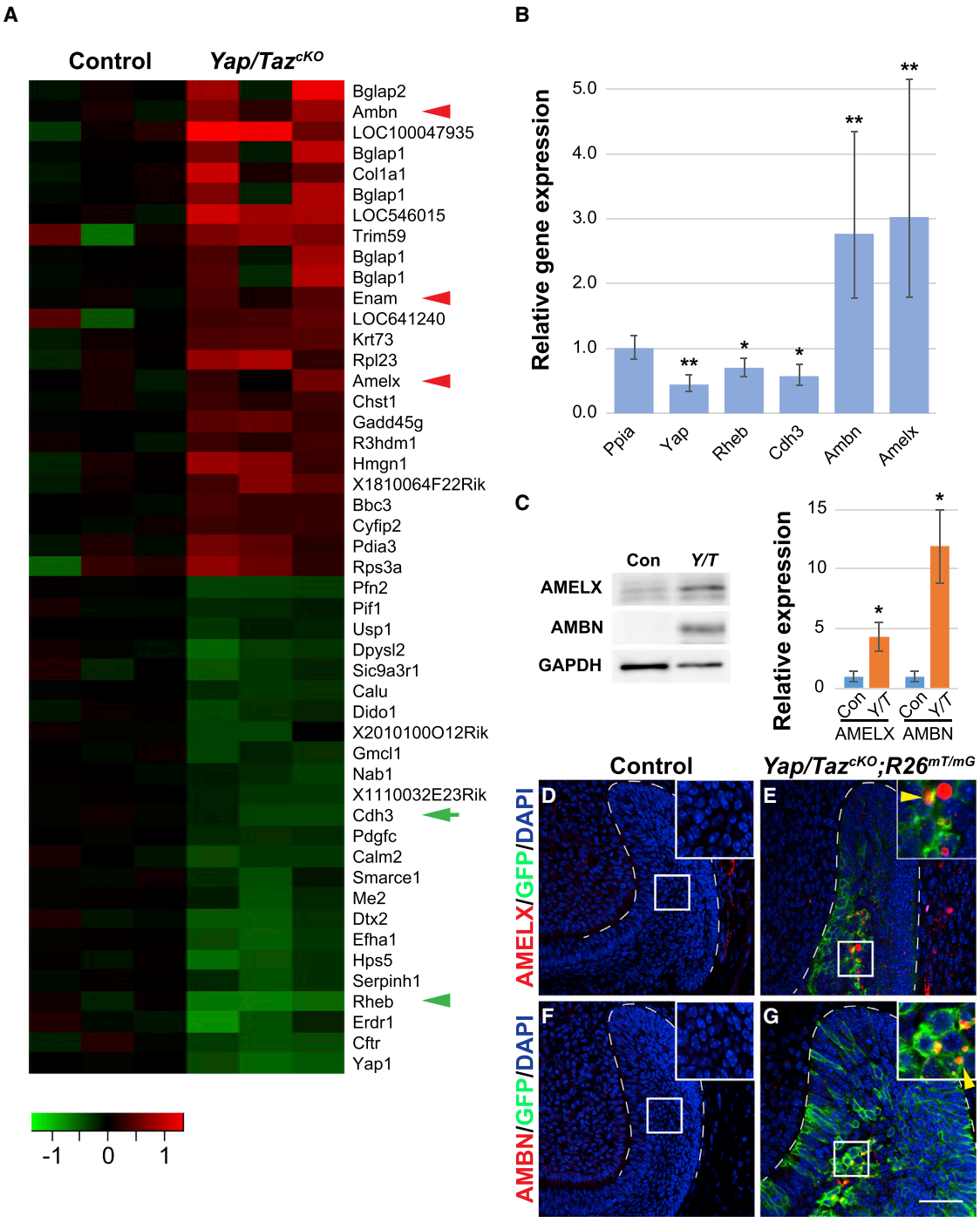

Figure 2. YAP/TAZ Inhibit Precocious Differentiation in the laCL

(A) Heatmap of up- and downregulated genes in control and *Yap/Taz*^{cKO} laCLs. Red arrowheads mark genes associated with ameloblast differentiation, and green arrow and arrowhead mark *Cdh3* and *Rheb*, respectively.

(B) The qPCR results comparing relative gene expression between control and *Yap/Taz*^{cKO} laCLs. Data are presented as mean ± SEM.

(C) Immunoblotting and relative expression (mean ± SD) of Amelogenin (AMELX) and Ameloblastin (AMBN) in control and *Yap/Taz*^{cKO} laCLs.

(D–G) Immunostaining of AMELX and AMBN in control (D and F) and *Yap/Taz*^{cKO} (E and G) laCLs. Yellow arrowheads mark ectopic AMELX and AMBN expression. Dashed lines outline laCLs. Representative images, cropped blots, and data are shown (*$p < 0.05$ and **$p < 0.01$). Scale bar (shown in G) represents 50 μm in (D)–(G). See also Figure S1.

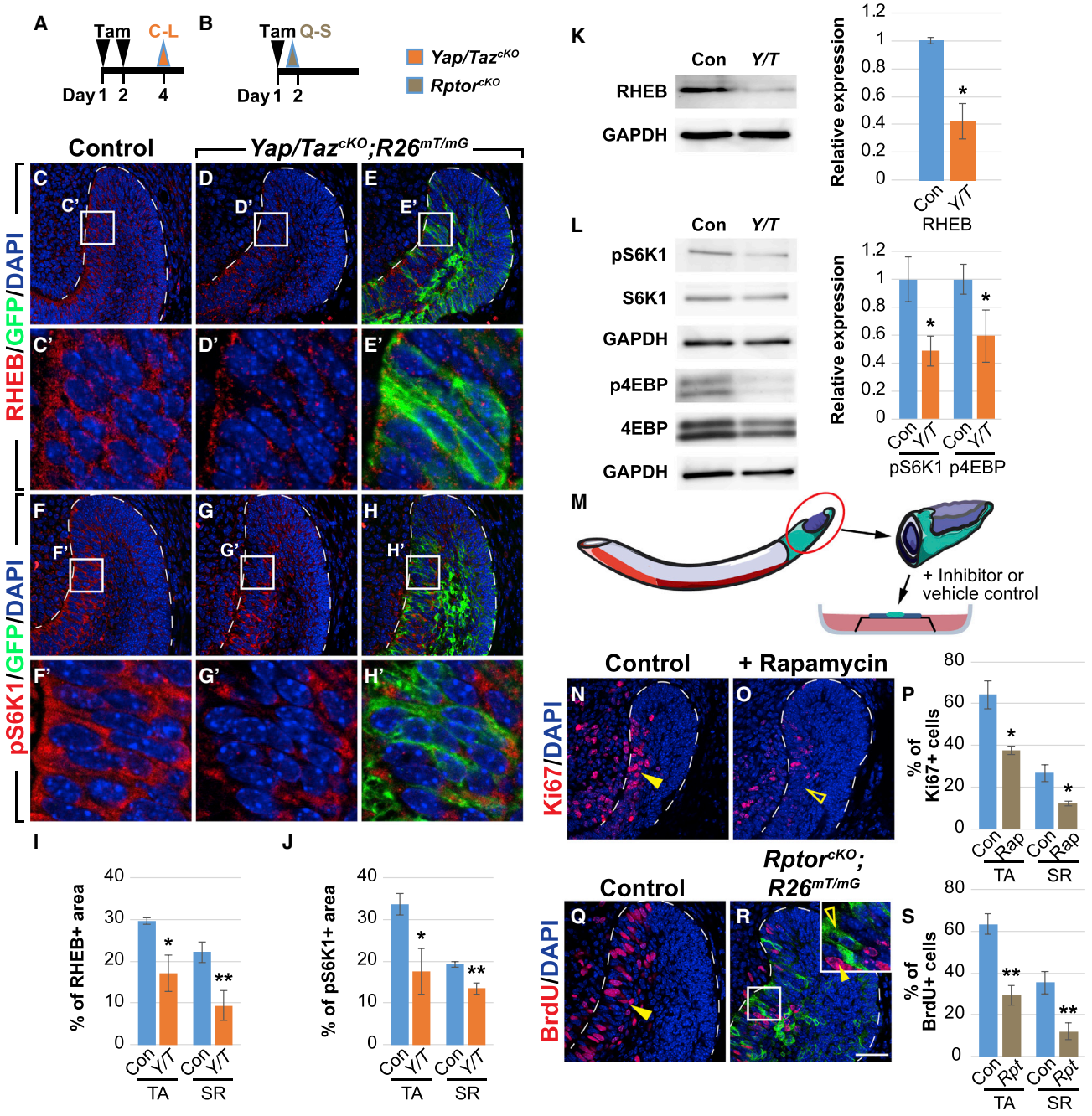

Figure 3. YAP/TAZ Are Required for *Rheb* Expression and mTOR Signaling

(A and B) Timelines indicating Cre induction (tamoxifen [Tam] injection, black arrowheads) and sample collection (orange and brown arrowheads) in *Yap/Taz*^{cKO} (A) and *Rptor*^{cKO} (B).

(C–J) RHEB (C–E') and pS6K1 (F–H') immunostaining in control and *Yap/Taz*^{cKO} laCLs. The percentage of RHEB- and pS6K1-positive area is quantified (I and J).

(K and L) Immunoblotting and relative expression of RHEB (K), pS6K1, and p4EBP (L).

(M) Schematic of the explant culture system.

(N–P) Ki67 expression in control (N) and Rapamycin-treated (O) explants. Closed and open arrowheads respectively mark normal and reduced proliferation. The percentage of Ki67-positive (+) cells per section is quantified (P).

(Q–S) BrdU labeling in control (Q) and *Rptor*^{cKO} (R) laCLs. Closed and open arrowheads mark normal and reduced proliferation in wild-type and mutant cells respectively. The percentage of BrdU-positive (+) cells per section is quantified (S).

Representative images, cropped blots, and quantitative data are shown. All quantitative data are presented as mean ± SD (*$p < 0.05$ and **$p < 0.01$). Dashed lines outline laCLs. Scale bar (shown in R) represents 50 μm in (C)–(E), (F)–(H), (N), (O), (Q), and (R) and 9.76 μm in (C′)–(E′) and (F′)–(H′). See also Figure S2.

carried out a small-scale screen using the explant culture system in combination with inhibitors of several known YAP regulators (Table S2). While most of the drugs tested did not affect YAP nuclear localization in TA cells (data not shown), the FAK inhibitor PF573228 impeded YAP accumulation in the nucleus (n = 12/12; Figures 4A and 4B), suggesting that integrin/FAK signaling may play a role in YAP regulation in the laCL (Figure 4F). Similarly, incisors treated with PP2, an inhibitor of SRC kinase that functions downstream of FAK, also had reduced nuclear YAP (n = 4/6; Figure 4C). Consistent with these results, immunostaining of phospho-FAK and -SRC (pFAK and pSRC) showed active FAK signaling in the TA region, but not in the OEE where there was low nuclear YAP (Figures 4D and 4E).

To further study whether FAK is required in the adult laCL for YAP nuclear localization, we deleted *Fak* in the dental epithelium by generating $K14^{CreER}$;$Fak^{f/f}$;$R26^{mT/mG}$ (Fak^{cKO}) mice. Similar to our explant studies, deletion of *Fak* resulted in loss of nuclear YAP in both TA and adjacent SR cells (Figures 4G–4J'). The reduction in nuclear YAP was quantified by calculating the percentage of YAP/DAPI overlap in control and Fak^{cKO} TA/SR cells (Figures 4K–4M), as well as by comparing the average nuclear YAP signal intensity both between control and mutant laCLs and between Cre-recombined (GFP-positive) and non-recombined (GFP-negative) cells in Fak^{cKO} (Figures S3A and S3B).

Having established FAK as an upstream regulator of YAP, we sought to find the corresponding integrin receptor by first screening the spatial distribution of potential integrin subunits that were expressed in the laCL based on our microarray data. We found that integrin α3 (ITGA3) was specifically expressed in the TA region and in the neighboring SR cells (Figure 4N). To investigate if ITGA3 functions upstream of YAP, we examined $K14^{Cre}$;$Itga3^{f/f}$ mice ($Itga3^{cKO}$), where *Itga3* was deleted in the entire dental epithelium (Figure 4O). In these mutants, there was a significant loss of nuclear YAP in TA cells, although SR cells were not affected (Figures 4P–4T and S3C). These data suggest that ITGA3 plays a dominant role in governing YAP localization in the TA region (Figure 4U), with other integrin subunits (such as ITGAV, which is present in the TA/SR regions as well; data not shown) performing similar functions in the SR. We also noted that, similar to Yap^{cKO}, both $Itga3^{cKO}$ and Fak^{cKO} laCLs appeared normal and had increased nuclear TAZ (Figures S4A–S4C' and S4E), reinforcing the notion that compensation by TAZ ensues following disrupted YAP activities. To test this, we generated Fak/Taz^{cKO} double mutants, and we found that laCLs from these animals had reduced proliferation 2 days after Cre induction and subsequently developed similar tissue loss as the Yap/Taz^{cKO} (n = 6/8; Figures S4F–S4O).

FAK Functions through CDC42 to Regulate YAP Localization

To investigate the mechanism by which FAK regulates YAP, we first focused on CDC42, a member of the small Rho GTPase family that also includes RHOA and RAC, which are key mediators of FAK signaling and whose functions can be modulated by the same pathway (McLean et al., 2005). Using an antibody against the active GTP-bound form of CDC42, we detected strong CDC42 activity in control TA and SR cells (Figures 5B and 5B'), while in Fak^{cKO} laCLs only sparse CDC42-GTP staining was observed (Figures 5A, 5C–5E, S3D, and S3E). This was corroborated by immunoprecipitation, which pulled down more active CDC42 from control laCLs than from Fak^{cKO} samples (Figure 5F), confirming that FAK is required for robust CDC42 activation. These experiments also point to the possibility that FAK regulates YAP localization through CDC42, and they predict that genetic ablation of CDC42 should phenocopy Fak^{cKO} and result in the loss of nuclear YAP. To that end, we genetically removed *Cdc42* in the dental epithelium using $K14^{CreER}$;$Cdc42^{f/f}$;$R26^{mT/mG}$ ($Cdc42^{cKO}$) mice, and we probed the expression of YAP using immunostaining. Confirming our hypothesis, YAP failed to accumulate in the nucleus in the absence of CDC42 (Figures 5G–5L, S3F, and S3G). Deletion of *Cdc42* also led to increased nuclear TAZ in the TA and inner SR regions (Figures S4D and S4E), consistent with what we observed in Fak^{cKO} and $Itga3^{cKO}$. Lastly, we note that deletion of *RhoA* and *Rac* or overexpression of a dominant-negative ROCK in laCLs did not affect YAP localization (data not shown). Collectively, these results reveal that FAK and CDC42 function within the same pathway to promote YAP nuclear localization in the laCL.

CDC42 Regulates YAP Phosphorylation at S397 through PP1A

To further understand the mechanism by which the FAK-CDC42 signaling axis regulates YAP localization, we examined the phosphorylation state of LATS, since the level of phospho-LATS (pLATS) reflects its ability to phosphorylate and inhibit YAP in many different systems (Zhao et al., 2007, 2010). Unexpectedly, we found that pLATS1 levels remained unchanged in the absence of CDC42 (Figure S5A), and we did not detect any alteration in the phosphorylation state of NDR1/2, which belong to the same NDR kinase family as LATS and have also been shown to phosphorylate YAP (Hergovich, 2016) (Figure S5B). Therefore, it is unlikely that CDC42 signals through LATS and NDR1/2 to regulate YAP in this context.

To more deeply investigate the mechanism underlying regulation of YAP localization by CDC42, we performed immunoblotting against pYAP-S127 and pYAP-S397. These phosphorylation sites are thought, based on cell culture experiments, to be critical for YAP cytoplasmic retention (S127) and protein stability (S397), respectively (Zhao et al., 2010). Interestingly, when compared to control laCLs, both $Cdc42^{cKO}$ and Fak^{cKO} laCLs showed an increase in pYAP-S397, but not pYAP-S127 (Figures 6A–6E), suggesting that signaling downstream of FAK and CDC42 preferentially controls YAP phosphorylation at S397.

This raised two possibilities, the first being that changes in YAP localization seen in $Cdc42^{cKO}$ laCLs are indirect results of pYAP-S397-driven YAP degradation, and the second being that pYAP-S397 has a yet-to-be-identified function in determining YAP localization. To address this, we utilized two mutant alleles of human *YAP*, $hYAP^{S127A}$ and $hYAP^{S397A}$, which can no longer be phosphorylated at those sites and, thus, are able to translocate to the nucleus even in the presence of an inhibitory signal. We then electroporated these constructs in the OEE (Figure 6F), where YAP is usually restricted to the cytoplasm (Figure 1D). When we electroporated the control *hYAP*, immunostaining using an antibody that only recognizes hYAP showed restriction to the OEE cytoplasm, as expected with wild-type YAP (Figure 6G). We next found that, while expression of YAP^{S127A} resulted in increased nuclear YAP, the number of cells

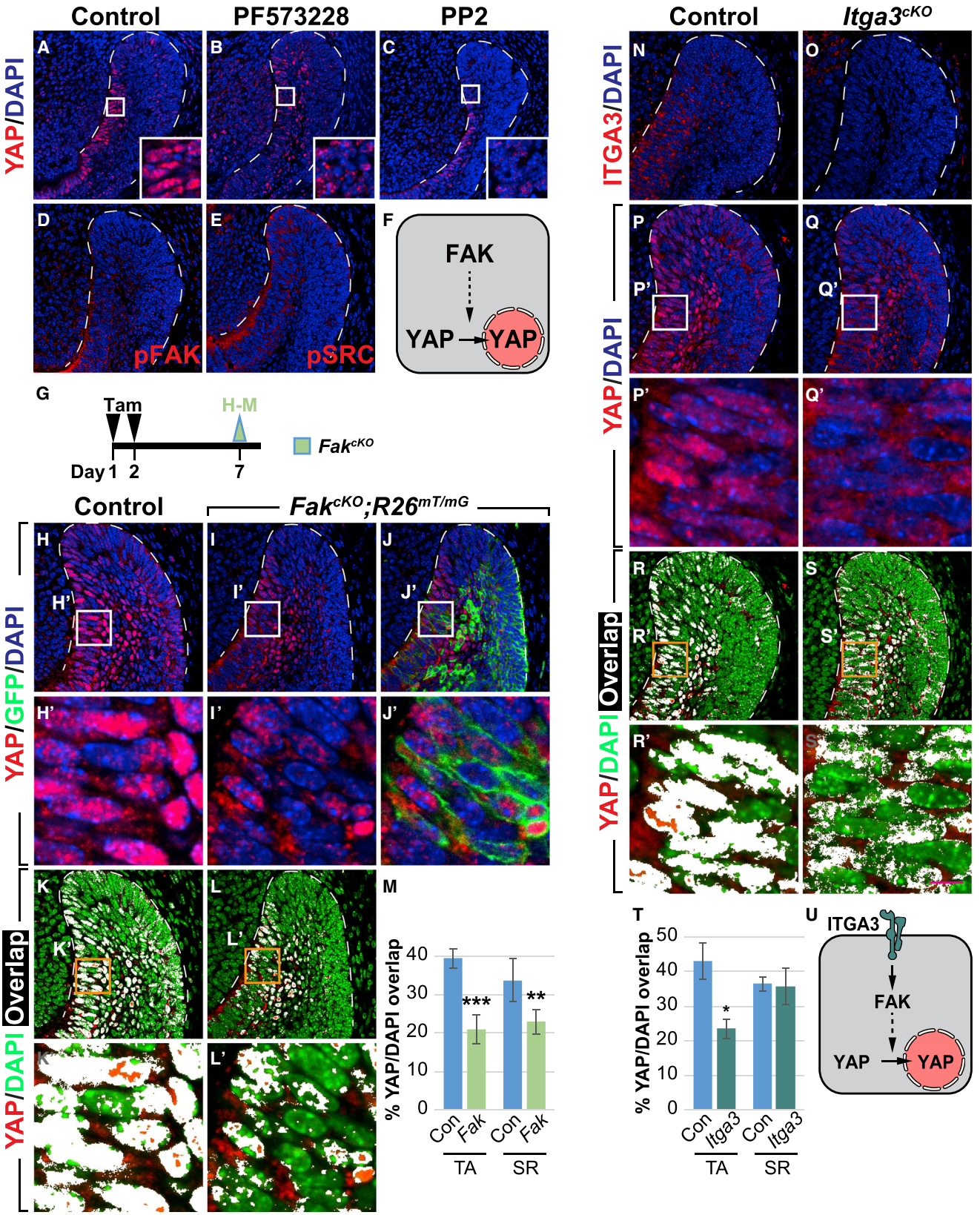

(legend on next page)

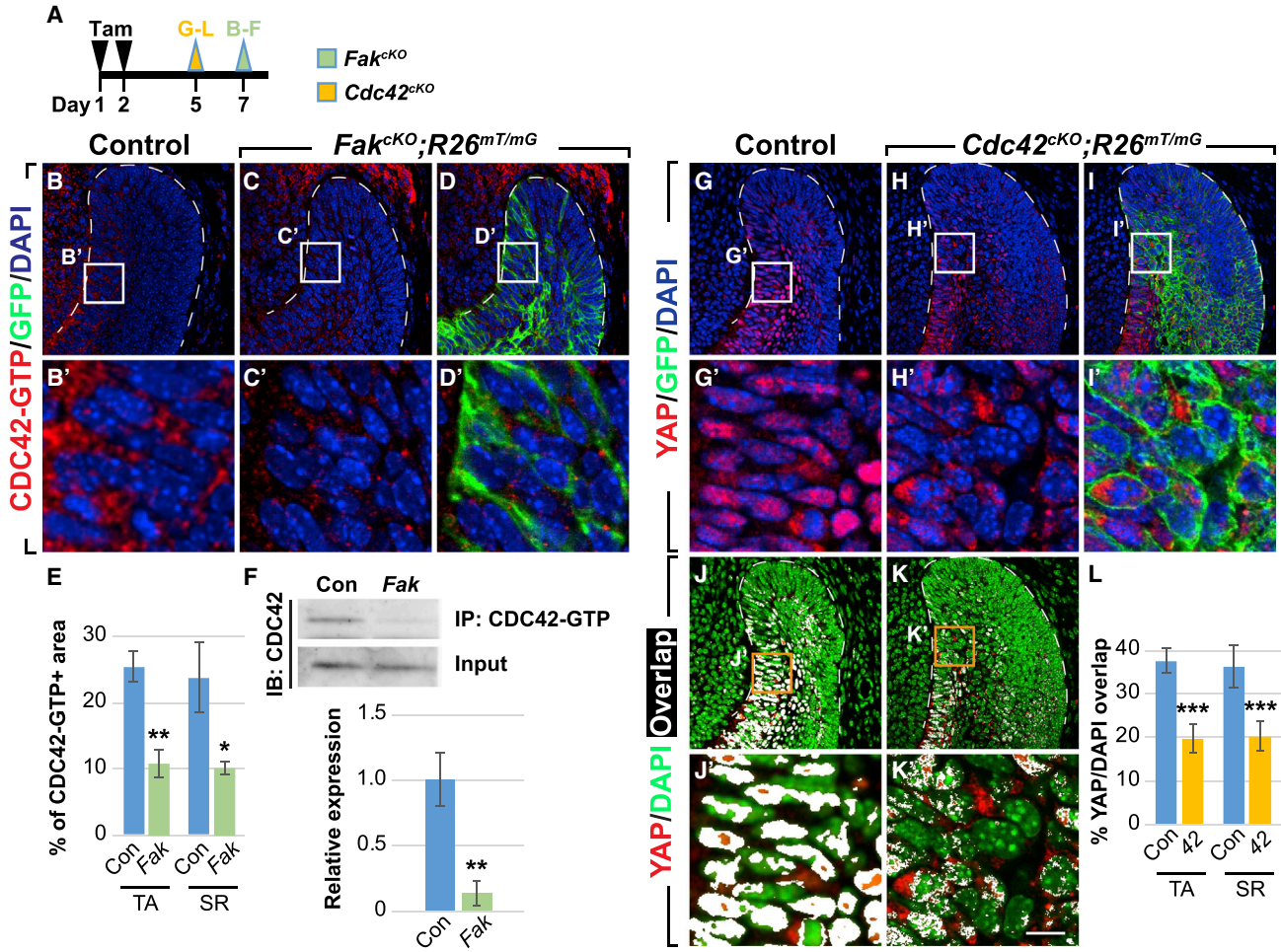

Figure 5. CDC42 Acts Downstream of FAK to Regulate YAP Nuclear Localization

(A) Timeline depicting tamoxifen (Tam) treatment (black arrowheads) and sample collection (green and yellow arrowheads).

(B–E) Immunostaining of active CDC42 in control (B and B′) and Fak^{cKO} (C–D′) laCLs. The percentage of area with positive CDC42-GTP staining is calculated (E).

(F) Immunoprecipitation of CDC42-GTP followed by CDC42 immunoblotting. Relative expression between control and Fak^{cKO} is quantified.

(G–L) YAP immunostaining in control (G and G′) and $Cdc42^{cKO}$ (H–I′) laCLs. The percentage of YAP/DAPI overlap is quantified (J–L).

Representative images, cropped blots, and quantitative data are shown. Data are presented as mean ± SD (*$p < 0.05$, **$p < 0.01$, and ***$p < 0.001$). Dashed lines outline laCLs. Scale bar (shown in K') represents 50 μm in (B)–(D), (G)–(I), (J), and (K) and 9.76 μm in (B′)–(D′), (G′)–(I′), (J′), and (K′). See also Figure S4.

with nuclear YAP and the YAP signal intensity were both lower than in $hYAP^{S397A}$-electroporated cells (Figures 6G–6I), pointing to YAP-S397 as the primary site for regulating YAP localization in the laCL. The outcome of YAP^{S127A} electroporation was also similar to genetic overexpression of YAP^{S127A} in laCLs, which was ineffective in driving YAP nuclear localization in the OEE (Figures S6A–S6C). Finally, $hYAP^{S127A,S397A}$ electroporation produced the highest nuclear YAP (Figures 6G–6I), highlighting the importance of both phosphorylation sites in controlling YAP localization.

Figure 4. ITGA3/FAK Signaling Promotes YAP Nuclear Localization in TA Cells

(A–C) YAP immunostaining in control (A), PF573228- and PP2-treated (B and C) explants.

(D and E) pFAK (D) and pSRC (E) expression in laCLs.

(F) Schematic diagram of a TA cell, where FAK promotes YAP nuclear localization.

(G) Timeline depicting tamoxifen (Tam) treatment (black arrowheads) and sample collection (green arrowhead).

(H–M) YAP immunostaining in control (H and H') and Fak^{cKO} (I–J′) laCLs. The percentage of YAP/DAPI overlap is quantified (K–M).

(N and O) ITGA3 expression in control (N) and $Itga3^{cKO}$ (O) laCLs.

(P–T) YAP immunostaining in control (P and P') and $Itga3^{cKO}$ (Q and Q′) laCLs. The percentage of YAP/DAPI overlap is quantified (R–T).

(U) Schematic diagram showing ITGA3/FAK signaling promotes nuclear YAP accumulation in TA cells.

Representative images and quantitative data are shown. All quantitative data are presented as mean ± SD (*$p < 0.05$, **$p < 0.01$, and ***$p < 0.001$). Dashed lines outline laCLs. Scale bar (shown in S′) represents 50 μm in (A)–(E), (H)–(J), (K), (L), (N)–(Q), (R), and (S) and 9.76 μm in (H′)–(J′), (K′), (L′), (P′), (Q′), (R′), and (S′). See also Figures S3 and S4.

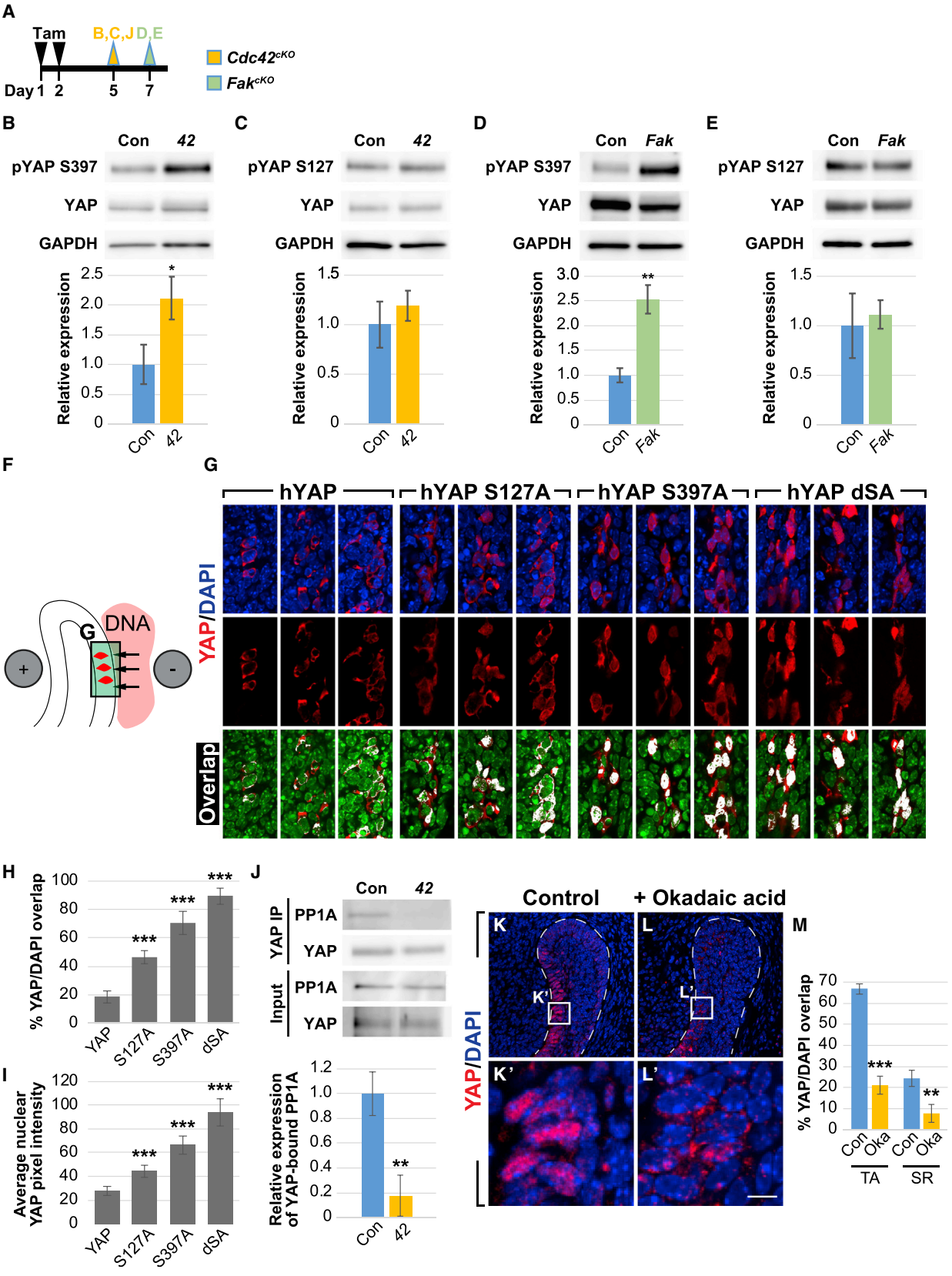

(legend on next page)

The preferential regulation at YAP-S397 also argues against a LATS-dependent mechanism downstream of FAK/CDC42, as LATS typically phosphorylates all YAP serine residues. Because PP1A may dephosphorylate YAP primarily on S397 (Qi et al., 2015), we tested whether PP1A binding to YAP was diminished upon *Cdc42* deletion. To that end, we performed co-immunoprecipitation of YAP and PP1A, and we found a significant reduction in pulled-down PP1A (but not PP2A, data not shown) in *Cdc42*^{cKO} laCL lysates (Figure 6J). This result then led to the prediction that PP1A is critical for activating YAP localization in the nucleus. Indeed, when cultured in the presence of okadaic acid, a PP1 inhibitor, incisor explants displayed a dramatic loss of nuclear YAP in TA cells (Figures 6K–6M and S3H), thus establishing an FAK/CDC42/PP1A signaling axis that governs YAP localization in the incisor TA cells.

LATS1/2 Function in Parallel to Regulate YAP Localization

The results above, however, could not rule out the possibility that LATS1/2 function in parallel to modulate YAP phosphorylation and activity, and this hypothesis was supported by the presence of abundant pYAP-S127 staining throughout the entire laCL (Figure S5D). To test this, we generated mice with *Lats1* and *Lats2* (*Lats1/2*^{cKO}) double deletions in the dental epithelium, and we observed a dramatic expansion of the dental epithelium in these mice 1 week after Cre activation (Figures 7A and 7B). Intriguingly, deletions of *Mst1* and *Mst2* did not result in any phenotype (Figures 7C, 7F, 7I, 7I', and S5I–S5K), indicating that LATS1/2 activity is regulated by other kinases, which could include MAP4K (Meng et al., 2015; Zheng et al., 2015). The hyperplasia seen in *Lats1/2*^{cKO} was limited to the TA region and the more distal ameloblasts, suggesting a differential response to the loss of *Lats1/2* in distinct cell types. This was corroborated by Ki67 staining, which showed only a marginal increase in the OEE but a striking upregulation in the more distal epithelium (Figures 7D and 7E). The expansion of proliferating cells was indicative of an enlarged TA region, and this was supported by the widespread expression of the TA marker P-cadherin (Li et al., 2012) throughout the distal epithelium (Figures S5E and S5F). Surprisingly, even though *Lats1/2*^{cKO} OEE was resistant to overproliferation, loss of *Lats1/2* resulted in increased nuclear YAP and the corresponding RHEB expression in the entire laCL (Figures 7G–7H', S5G, and S5H), supporting the notion that nuclear accumulation of YAP is not always sufficient to drive cell proliferation (Chen et al., 2015). Thus, these experiments revealed that LATS1/2 are required in the laCL to restrain uncontrolled YAP activity and may do so in parallel to the FAK-CDC42 signaling axis described above.

DISCUSSION

The homeostatic maintenance of self-renewing tissues depends on a continuous supply of differentiated cells from resident somatic stem cells. Using the adult mouse incisor as a model, we have uncovered a novel signaling network regulating TA cell proliferation and differentiation. Our data support a framework (Figure 7J) in which local induction of the integrin-FAK-CDC42 signaling axis modulates YAP phosphorylation at S397 to control YAP localization and activity, which in turn govern progenitor cell proliferation and differentiation by means of transcriptional regulation of downstream effectors, such as RHEB. This pathway is counterbalanced by LATS activity and can be compensated by the functionally redundant TAZ. As a consequence, a robust system is in place that can be tuned to ensure adequate production of new cells, in order to meet the homeostatic demand of the tissue, and support continuous growth of the tooth, which is critical for the survival of the animal.

Maintenance of Progenitor Cells by YAP/TAZ

In this study, we identified YAP/TAZ as key regulators of mouse incisor renewal that promote TA cell proliferation, prevent apoptosis, inhibit precocious differentiation in dental progenitor cells, and maintain the overall structure of the tissue. This finding thus provides a mechanism for regulating the expansion of progenitor cells during continuous tissue renewal, and it resonates with a growing body of work on the roles of YAP/TAZ in stem/progenitor cells (Yu et al., 2015). Interestingly, the requirement for YAP/TAZ in tissue homeostasis differs among organs. For instance, while YAP is indispensable for cell proliferation in the skin (Schlegelmilch et al., 2011), the mammary gland and intestine remain relatively normal after *Yap* deletion (Cai et al., 2010; Chen et al., 2014). Similarly, although *Taz* is essential for kidney and lung development (Makita et al., 2008; Reginensi et al., 2013), it is functionally redundant with YAP during heart and craniofacial development (Wang et al., 2016; Xin et al., 2011). Here we found that YAP/TAZ have overlapping functions in the adult incisor, and ablation of *Yap*/*Taz* had a profound impact on the maintenance of laCLs, especially the TA and SR regions. The eventual loss of the entire laCL in the *Yap*/*Taz*^{cKO} is due to either an absolute dependence of OEE cells on TA/SR cells or on a yet-to-be-identified role of YAP in the OEE cytoplasm. One potential cytoplasmic function of YAP/TAZ to be explored in the future is engagement in WNT signaling (Varelas et al., 2010), although the WNT pathway does not appear to be active in the laCL (Suomalainen and Thesleff, 2010).

Our analysis of *Lats*^{cKO} laCLs also revealed differences between TA cells and DESCs/OEE cells in response to increased

Figure 6. CDC42 Signals through PP1A to Regulate YAP S397 Phosphorylation and Localization

(A) Timeline indicating tamoxifen (Tam) injection (black arrowheads) and sample collection (green and yellow arrowheads).

(B–E) Immunoblotting and relative expression of pYAP-S397 and pYAP-S127 in control, *Cdc42*^{cKO} (B and C), and *Fak*^{cKO} (D and E) laCLs.

(F) Schematic diagram depicting delivery of YAP constructs to the OEE by electroporation.

(G–I) YAP immunostaining and YAP/DAPI overlap in explants electroporated with hYAP, hYAP-S127A, hYAP-S397A, and hYAP-S127A,S397A (hYAP-dSA) in the OEE (G). Three representative images are shown for each construct. The percentage of YAP/DAPI overlap (H) and average nuclear YAP pixel intensity (I) are quantified.

(J) YAP immunoprecipitation followed by PP1A detection. Relative expression of PP1A between control and *Cdc42*^{cKO} is displayed.

(K–M) YAP immunostaining in control (K and K′) and okadaic acid-treated (L and L′) laCLs. The percentage of YAP/DAPI overlap is calculated (M).

Representative images, cropped blots, and quantitative data are shown. Dashed lines outline laCLs. Scale bar (shown in L′) represents 15 μm in (G), 50 μm in (K) and (L), and 9.76 μm in (K′) and (L′). All data are presented as mean ± SD (*$p < 0.05$, **$p < 0.01$, and ***$p < 0.001$). See also Figures S3, S5, and S6.

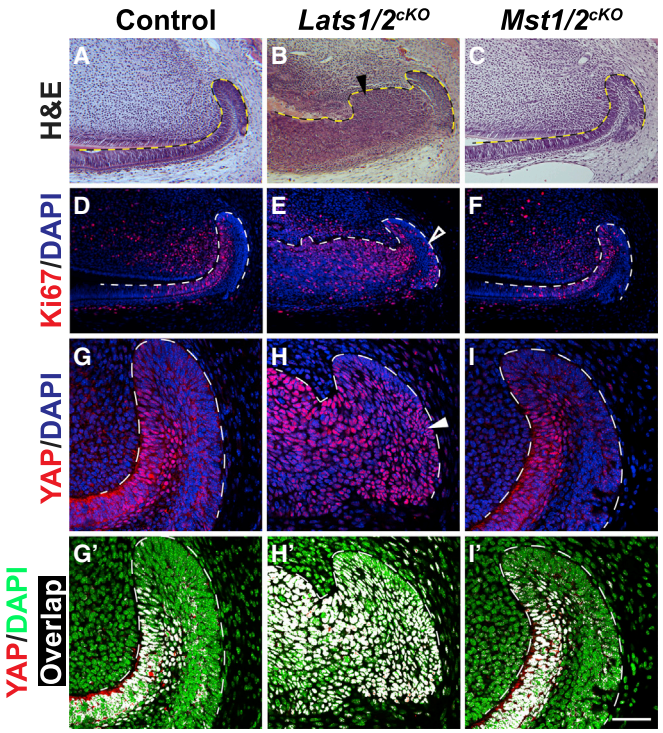

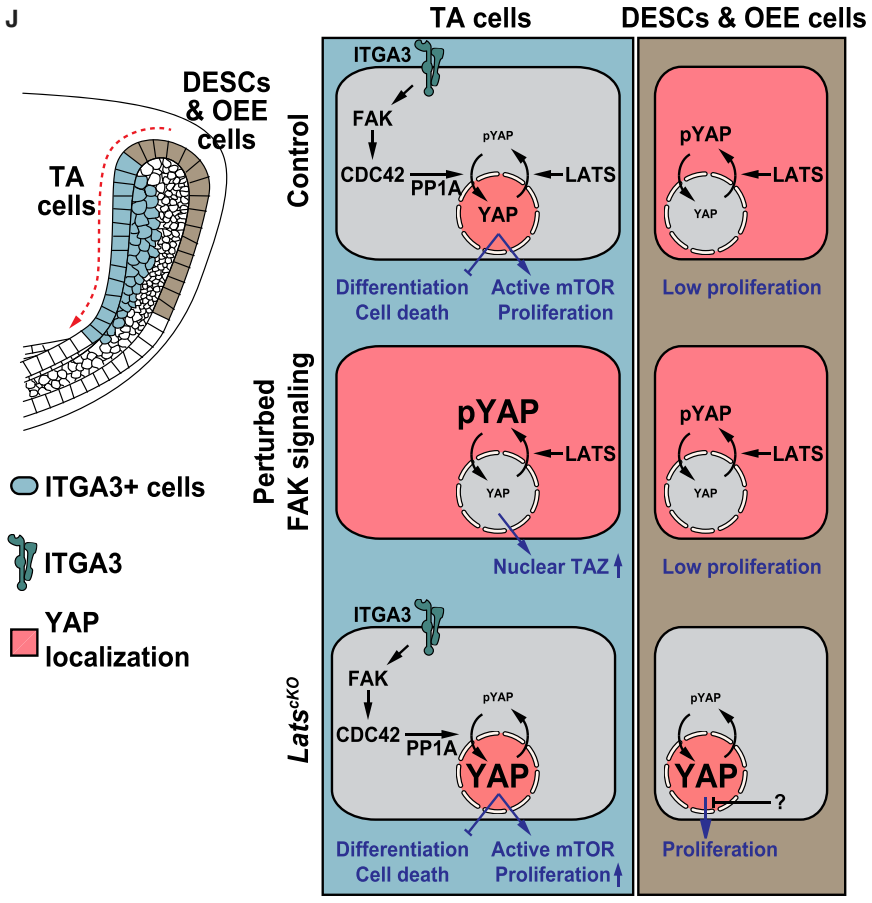

Figure 7. LATS1/2 Are Required to Prevent Tissue Hyperplasia in the laCL and a Model for YAP-Mediated Incisor Renewal

(A–C) H&E staining of control (A), *Lats1/2*^{cKO} (B), and *Mst1/2*^{cKO} (C) proximal incisors. Arrowhead in (B) marks tissue hyperplasia.

(D–F) Ki67 expression in control (D), *Lats1/2*^{cKO} (E), and *Mst1/2*^{cKO} (F) dental epithelium. Open arrowhead in (E) marks the few proliferating cells in *Lats1/2*^{cKO} OEE.

(G–I′) YAP immunostaining and YAP/DAPI overlap in control (G and G′), *Lats1/2*^{cKO} (H and H′), and *Mst1/2*^{cKO} (I and I′) laCLs. Arrowhead in (H) marks increased nuclear YAP in *Lats1/2*^{cKO}.

(J) Model for the regulation of incisor stem cell-based dental renewal. ITGA3-positive TA and inner SR cells are marked blue and DESCs/OEE cells are marked brown. Red shade represents YAP localization. In control TA cells, an ITGA3/FAK/CDC42/PP1A signaling axis drives YAP nuclear localization, which promotes proliferation by activating mTOR signaling and inhibits precocious differentiation and apoptosis. When FAK signaling is perturbed, loss of nuclear YAP is compensated for by increased nuclear TAZ. In parallel, LATS1/2 fine-tune levels of nuclear YAP to prevent over-proliferation. In contrast to TA cells, DESCs/OEE cells are relatively inert and are resistant to YAP-driven proliferation.

Representative images and quantitative data are shown. Dashed lines outline the dental epithelium. Scale bar (shown in I′) represents 130 μm in (A)–(F) and 50 μm in (G)–(I′). See also Figure S5.

nuclear YAP, as TA cells expanded into a multilayered structure upon *Lats1/2* deletion, and DESCs/OEE cells were resistant to nuclear YAP-induced overproliferation. This thus points to the possibility that nuclear YAP acts as a permissive signal and that additional stimuli must be in place to drive proliferation. One candidate for such signals are the FGFs secreted from the mesenchyme overlying the TA cells. Attenuation of FGFR2b signaling in the dental epithelium impeded TA cell proliferation, and increased FGF signaling, due to the loss of *Sprouty* genes, transformed the low-proliferating lingual CL into an laCL equivalent (Klein et al., 2008; Parsa et al., 2010). Indeed, FGF signaling has been shown to be required for YAP-induced proliferation in other contexts (Hua et al., 2016). Alternatively, the presence of nuclear YAP in $Lats^{cKO}$ OEE cells is counterbalanced by a compensatory decrease in the overall YAP protein level (Chen et al., 2015). Finally, cells in the OEE are more densely clustered than TA cells, and they express cell adhesion molecules, such as E-cadherin and Claudin1, that are absent in TA cells (Li et al., 2012) and may add further control over cell proliferation.

Regulation of YAP by Integrin/FAK Signaling in Progenitor Cells

An important question in the field of Hippo signaling and stem cell biology is understanding how YAP activity is triggered to promote the expansion of tissue progenitors. We found that this is achieved in the incisor by restricted expression of ITGA3 and the corresponding activation of FAK signaling in the TA region, which subsequently promotes YAP nuclear localization through CDC42. Regulation of YAP by FAK signaling has been recently observed in other stem cell systems, including skeletal and epithelial stem cells (Elbediwy et al., 2016; Tang et al., 2013). However, in these cases, RHOA was placed downstream of FAK, and CDC42 was instead an inhibitory signal through its role in apical polarity formation. The differences could be due to the use of distinct experimental models, as previous results were derived from cell culture studies. Along these lines, CDC42 is an essential regulator of YAP during kidney development and for podocyte survival, while deletion of *RhoA* and *Rac* had little effect (Huang et al., 2016; Reginensi et al., 2013), suggesting that CDC42 may be the predominant Rho GTPase for YAP regulation in vivo.

We also noted that YAP and TAZ are differentially regulated in the laCL, with TAZ being a compensatory effector when YAP or FAK activity is disrupted. This is similar to an earlier study, where hepatic or intestinal deletion of *Yap* resulted in TAZ nuclear localization (Moroishi et al., 2015), demonstrating that TAZ can function as a reserve pool in vivo that becomes activated in response to *Yap* loss. Indeed, deletion of both *Fak* and *Taz* phenocopies Yap/Taz^{cKO}, although with a milder phenotype, likely due to residual nuclear YAP in some cells.

Another critical aspect of the ITGA3/FAK/CDC42 signaling axis is that it is independent of LATS activity. Instead, we identified PP1A as an important modulator of YAP phosphorylation downstream of CDC42. PP1A itself could potentially be activated by the CDC42 effector PAK2 (Zhang et al., 2013), and PAK2 activity was reduced in $Cdc42^{cKO}$ laCLs (Figure S5C). Interestingly, ITGA3/FAK/CDC42 signaling predominantly controls YAP phosphorylation at S397, but not S127, a phenomenon that has been previously shown in Netrin-1-induced PP1A dephosphorylation of YAP (Qi et al., 2015). As S397 phosphorylation affects YAP stability in vitro (Zhao et al., 2010), it is possible that, in the laCL, FAK signaling modulates YAP localization indirectly by maintaining YAP protein levels above a certain threshold. However, as YAP levels were comparable in control, Fak^{cKO} and $Cdc42^{cKO}$ laCLs, an alternative explanation is that pYAP-S397 directly contributes to YAP localization. This is supported by two observations as follows: first, overexpression of YAP^{S127A} did not result in an efficient upregulation of nuclear YAP in the laCL, and, second, electroporation of an $hYAP^{S127A,S397A}$ construct resulted in higher nuclear YAP localization than YAP^{S127A}. Taken together, our results indicate that the ITGA3/FAK/CDC42 signaling axis functions in parallel to LATS to promote nuclear YAP localization through dephosphorylation at YAP-S397.

The signaling axis described here likely functions in other stem cell settings as well, as integrin/FAK signaling is prevalent in many different stem cell niches and is critical for maintaining cell proliferation, preserving the stem cell population and balancing renewal and differentiation (Prowse et al., 2011). For instance, conditional deletion of β1 integrin in the skin results in severe reduction of proliferation (Raghavan et al., 2000), whereas heightened integrin signaling potentiates cancer stem cell activities (Seguin et al., 2015). Indeed, α3β1 is crucial for promoting proliferation and tumor growth in skin cancers (Sachs et al., 2012), and it is plausible that YAP acts downstream of the aberrant signaling, as well as in other normal or pathological conditions where integrin signaling plays a role.

Transcriptional Outputs of YAP/TAZ

The role of YAP/TAZ in transcriptional regulation has been well characterized (Yu et al., 2015), and in the incisor we found that YAP/TAZ facilitate TA cell expansion in part through their control of *Rheb* expression and, thus, mTOR activity. As a central effector of cell growth and proliferation, mTOR signaling has also been shown to mediate YAP function elsewhere (Hansen et al., 2015; Tumaneng et al., 2012), and our data add to the growing evidence that YAP is able to induce mTOR signaling through several different pathways.

Importantly, both Rapamycin-treated and $Rptor^{cKO}$ laCLs did not present any obvious loss of cell-cell adhesion analogous to what we observed in Yap/Taz^{cKO}, suggesting that additional downstream genes were responsible for the cell adhesion phenotype. One potential candidate is the cell adhesion molecule P-cadherin (encoded by *Cdh3*), which was downregulated both at the RNA and protein levels (Figures 2B and S2O–S2R) along with other genes, such as *Serpinh1*, *Dpysl2*, and *Pfn2*, that are also important for cytoskeletal regulation (Figure 2A). As a result, YAP/TAZ may maintain tissue integrity by controlling the expression of these genes to modulate cellular tension and extracellular matrix (ECM) environment, in line with a recent finding in zebrafish (Porazinski et al., 2015).

Finally, YAP/TAZ are critical for inhibiting the expression of genes that are associated with differentiated cells. In Yap/Taz^{cKO} laCLs, activation of these genes primarily occurs in SR cells, likely because these cells are further along in the differentiation process and, therefore, more sensitive to the loss of YAP/TAZ. It is currently unknown whether YAP/TAZ directly regulate the expression of these genes, and it will be important to address

this in future experiments and in other tissues, which may shed light on how YAP/TAZ govern the balance between stem cell proliferation and differentiation. Taken together, these studies have uncovered a novel FAK-YAP-mTOR signaling pathway that governs proliferation and differentiation in tissue progenitor cells. This work helps to provide a framework for future research into the roles of integrins and YAP in both normal and pathological conditions, as well as to develop strategies for stem cell-based regeneration of dental and other mineralized tissues.

STAR★METHODS

Detailed methods are provided in the online version of this paper and include the following:

- KEY RESOURCES TABLE
- CONTACT FOR REAGENT AND RESOURCE SHARING
- EXPERIMENTAL MODEL AND SUBJECT DETAILS
  - Mouse lines and induction of alleles
  - Sample sources for laCL cells and explants
- METHOD DETAILS
  - Tissue preparation and histological analysis
  - Immunofluorescence staining
  - In situ hybridization
  - Microtomography
  - Isolation of laCLs
  - Explant culture
  - Electroporation
  - Colony formation assay
  - Western blot and immunoprecipitation
  - Expression profiling by microarray
  - qPCR analysis
- STATISTICAL ANALYSIS
  - Statistics
  - ImageJ image analysis
- DATA AVAILABILITY

SUPPLEMENTAL INFORMATION

Supplemental Information includes six figures and five tables and can be found with this article online at http://dx.doi.org/10.1016/j.stem.2017.03.023.

AUTHOR CONTRIBUTIONS

Conceptualization, J.K.-H.H. and O.D.K.; Methodology, J.K.-H.H. and O.D.K.; Investigation, J.K.-H.H., W.D., and C.M.D.; Formal Analysis, S.J.S.; Writing – Original Draft, J.K.-H.H. and O.D.K.; Writing – Review & Editing, J.K.-H.H. and O.D.K.; Resources, C.M.D.; Funding Acquisition, J.K.-H.H., M.C.O., C.M.D., and O.D.K.; Supervision, O.D.K.

ACKNOWLEDGMENTS

We thank Sarah Alto, Rebecca d'Urso, and Nicholas Wang for assistance with the mouse colony; Dr. Amnon Sharir for help with μCT imaging; Derek Power for technical assistance; Drs. Anandika Aggarwal, Aaditi Mujumdar, and Chandana Vundavalli for assistance with sample preparation; members of the Klein laboratory, Dr. Jeffrey Bush, and Dr. Valerie Weaver for helpful discussions; and Drs. Eric Olson, Randy Johnson, Louis Reichardt, Fernando Camargo, and Cord Brakebusch and RIKEN BRC for mouse lines. This work was funded by NIDCR R01-DE024988 and R35-DE026602 to O.D.K. and F32-DE023705 and K99-DE025874 to J.K.-H.H.

Received: October 10, 2016
Revised: February 7, 2017
Accepted: March 26, 2017
Published: April 27, 2017

REFERENCES

Aggarwal, A., Al-Rohil, R.N., Batra, A., Feustel, P.J., Jones, D.M., and DiPersio, C.M. (2014). Expression of integrin α3β1 and cyclooxygenase-2 (COX2) are positively correlated in human breast cancer. BMC Cancer *14*, 459.

Bai, H., Zhang, N., Xu, Y., Chen, Q., Khan, M., Potter, J.J., Nayar, S.K., Cornish, T., Alpini, G., Bronk, S., et al. (2012). Yes-associated protein regulates the hepatic response after bile duct ligation. Hepatology *56*, 1097–1107.

Baldi, P., and Long, A.D. (2001). A Bayesian framework for the analysis of microarray expression data: regularized t -test and statistical inferences of gene changes. Bioinformatics *17*, 509–519.

Beggs, H.E., Schahin-Reed, D., Zang, K., Goebbels, S., Nave, K.A., Gorski, J., Jones, K.R., Sretavan, D., and Reichardt, L.F. (2003). FAK deficiency in cells contributing to the basal lamina results in cortical abnormalities resembling congenital muscular dystrophies. Neuron *40*, 501–514.

Benjamini, Y., and Hochberg, Y. (1995). Controlling the false discovery rate: a practical and powerful approach to multiple testing. J. R. Stat. Soc. Series B (Methodological) *57*, 289–300.

Biehs, B., Hu, J.K., Strauli, N.B., Sangiorgi, E., Jung, H., Heber, R.P., Ho, S., Goodwin, A.F., Dasen, J.S., Capecchi, M.R., and Klein, O.D. (2013). BMI1 represses Ink4a/Arf and Hox genes to regulate stem cells in the rodent incisor. Nat. Cell Biol. *15*, 846–852.

Cai, J., Zhang, N., Zheng, Y., de Wilde, R.F., Maitra, A., and Pan, D. (2010). The Hippo signaling pathway restricts the oncogenic potential of an intestinal regeneration program. Genes Dev. *24*, 2383–2388.

Camargo, F.D., Gokhale, S., Johnnidis, J.B., Fu, D., Bell, G.W., Jaenisch, R., and Brummelkamp, T.R. (2007). YAP1 increases organ size and expands undifferentiated progenitor cells. Curr. Biol. *17*, 2054–2060.

Chen, T., Heller, E., Beronja, S., Oshimori, N., Stokes, N., and Fuchs, E. (2012). An RNA interference screen uncovers a new molecule in stem cell self-renewal and long-term regeneration. Nature *485*, 104–108.

Chen, Q., Zhang, N., Gray, R.S., Li, H., Ewald, A.J., Zahnow, C.A., and Pan, D. (2014). A temporal requirement for Hippo signaling in mammary gland differentiation, growth, and tumorigenesis. Genes Dev. *28*, 432–437.

Chen, Q., Zhang, N., Xie, R., Wang, W., Cai, J., Choi, K.-S., David, K.K., Huang, B., Yabuta, N., Nojima, H., et al. (2015). Homeostatic control of Hippo signaling activity revealed by an endogenous activating mutation in YAP. Genes Dev. *29*, 1285–1297.

Damljanović, V., Lagerholm, B.C., and Jacobson, K. (2005). Bulk and micropatterned conjugation of extracellular matrix proteins to characterized polyacrylamide substrates for cell mechanotransduction assays. Biotechniques *39*, 847–851.

Dassule, H.R., Lewis, P., Bei, M., Maas, R., and McMahon, A.P. (2000). Sonic hedgehog regulates growth and morphogenesis of the tooth. Development *127*, 4775–4785.

Dupont, S., Morsut, L., Aragona, M., Enzo, E., Giulitti, S., Cordenonsi, M., Zanconato, F., Le Digabel, J., Forcato, M., Bicciato, S., et al. (2011). Role of YAP/TAZ in mechanotransduction. Nature *474*, 179–183.

Elbediwy, A., Vincent-Mistiaen, Z.I., Spencer-Dene, B., Stone, R.K., Boeing, S., Wculek, S.K., Cordero, J., Tan, E.H., Ridgway, R., Brunton, V.G., et al. (2016). Integrin signalling regulates YAP and TAZ to control skin homeostasis. Development *143*, 1674–1687.

Glogauer, M., Marchal, C.C., Zhu, F., Worku, A., Clausen, B.E., Foerster, I., Marks, P., Downey, G.P., Dinauer, M., and Kwiatkowski, D.J. (2003). Rac1 deletion in mouse neutrophils has selective effects on neutrophil functions. J. Immunol. *170*, 5652–5657.

Hansen, C.G., Ng, Y.L.D., Lam, W.-L.M., Plouffe, S.W., and Guan, K.-L. (2015). The Hippo pathway effectors YAP and TAZ promote cell growth by modulating amino acid signaling to mTORC1. Cell Res. *25*, 1299–1313.

Hara, K., Maruki, Y., Long, X., Yoshino, K., Oshiro, N., Hidayat, S., Tokunaga, C., Avruch, J., and Yonezawa, K. (2002). Raptor, a binding partner of target of rapamycin (TOR), mediates TOR action. Cell *110*, 177–189.

Harada, H., Kettunen, P., Jung, H.S., Mustonen, T., Wang, Y.A., and Thesleff, I. (1999). Localization of putative stem cells in dental epithelium and their association with Notch and FGF signaling. J. Cell Biol. *147*, 105–120.

Hay, N., and Sonenberg, N. (2004). Upstream and downstream of mTOR. Genes Dev. *18*, 1926–1945.

Heallen, T., Zhang, M., Wang, J., Bonilla-Claudio, M., Klysik, E., Johnson, R.L., and Martin, J.F. (2011). Hippo pathway inhibits Wnt signaling to restrain cardiomyocyte proliferation and heart size. Science *332*, 458–461.

Hergovich, A. (2016). The Roles of NDR Protein Kinases in Hippo Signalling. Genes (Basel) *7*, E21.

Hua, G., Lv, X., He, C., Remmenga, S.W., Rodabough, K.J., Dong, J., Yang, L., Lele, S.M., Yang, P., Zhou, J., et al. (2016). YAP induces high-grade serous carcinoma in fallopian tube secretory epithelial cells. Oncogene *35*, 2247–2265.

Huang, Z., Zhang, L., Chen, Y., Zhang, H., Zhang, Q., Li, R., Ma, J., Li, Z., Yu, C., Lai, Y., et al. (2016). Cdc42 deficiency induces podocyte apoptosis by inhibiting the Nwasp/stress fibers/YAP pathway. Cell Death Dis. *7*, e2142.

Jackson, B., Peyrollier, K., Pedersen, E., Basse, A., Karlsson, R., Wang, Z., Lefever, T., Ochsenbein, A.M., Schmidt, G., Aktories, K., et al. (2011). RhoA is dispensable for skin development, but crucial for contraction and directed migration of keratinocytes. Mol. Biol. Cell *22*, 593–605.

Johnson, W.E., Li, C., and Rabinovic, A. (2007). Adjusting batch effects in microarray expression data using empirical Bayes methods. Biostatistics *8*, 118–127.

Juuri, E., Saito, K., Ahtiainen, L., Seidel, K., Tummers, M., Hochedlinger, K., Klein, O.D., Thesleff, I., and Michon, F. (2012). Sox2+ stem cells contribute to all epithelial lineages of the tooth via Sfrp5+ progenitors. Dev. Cell *23*, 317–328.

Kaukua, N., Shahidi, M.K., Konstantinidou, C., Dyachuk, V., Kaucka, M., Furlan, A., An, Z., Wang, L., Hultman, I., Ährlund-Richter, L., et al. (2014). Glial origin of mesenchymal stem cells in a tooth model system. Nature *513*, 551–554.

Kayala, M.A., and Baldi, P. (2012). Cyber-T web server: differential analysis of high-throughput data. Nucleic Acids Res. *40*, W553–559.

Klein, O.D., Lyons, D.B., Balooch, G., Marshall, G.W., Basson, M.A., Peterka, M., Boran, T., Peterkova, R., and Martin, G.R. (2008). An FGF signaling loop sustains the generation of differentiated progeny from stem cells in mouse incisors. Development *135*, 377–385.

Kobayashi, K., Takahashi, M., Matsushita, N., Miyazaki, J., Koike, M., Yaginuma, H., Osumi, N., Kaibuchi, K., and Kobayashi, K. (2004). Survival of developing motor neurons mediated by Rho GTPase signaling pathway through Rho-kinase. J. Neurosci. *24*, 3480–3488.

Lange, A.W., Sridharan, A., Xu, Y., Stripp, B.R., Perl, A.-K., and Whitsett, J.A. (2015). Hippo/Yap signaling controls epithelial progenitor cell proliferation and differentiation in the embryonic and adult lung. J. Mol. Cell Biol. *7*, 35–47.

Laplante, M., and Sabatini, D.M. (2009). mTOR signaling at a glance. J. Cell Sci. *122*, 3589–3594.

Levy, D., Adamovich, Y., Reuven, N., and Shaul, Y. (2008). Yap1 phosphorylation by c-Abl is a critical step in selective activation of proapoptotic genes in response to DNA damage. Mol. Cell *29*, 350–361.

Li, M., Indra, A.K., Warot, X., Brocard, J., Messaddeq, N., Kato, S., Metzger, D., and Chambon, P. (2000). Skin abnormalities generated by temporally controlled RXRalpha mutations in mouse epidermis. Nature *407*, 633–636.

Li, C.-Y., Cha, W., Luder, H.-U., Charles, R.-P., McMahon, M., Mitsiadis, T.A., and Klein, O.D. (2012). E-cadherin regulates the behavior and fate of epithelial stem cells and their progeny in the mouse incisor. Dev. Biol. *366*, 357–366.

Li, P., Silvis, M.R., Honaker, Y., Lien, W.-H., Arron, S.T., and Vasioukhin, V. (2016). αE-catenin inhibits a Src-YAP1 oncogenic module that couples tyrosine kinases and the effector of Hippo signaling pathway. Genes Dev. *30*, 798–811.

Livak, K.J., and Schmittgen, T.D. (2001). Analysis of relative gene expression data using real-time quantitative PCR and the 2(-Delta Delta C(T)) Method. Methods *25*, 402–408.

Lu, L., Li, Y., Kim, S.M., Bossuyt, W., Liu, P., Qiu, Q., Wang, Y., Halder, G., Finegold, M.J., Lee, J.-S., and Johnson, R.L. (2010). Hippo signaling is a potent in vivo growth and tumor suppressor pathway in the mammalian liver. Proc. Natl. Acad. Sci. USA *107*, 1437–1442.

Makita, R., Uchijima, Y., Nishiyama, K., Amano, T., Chen, Q., Takeuchi, T., Mitani, A., Nagase, T., Yatomi, Y., Aburatani, H., et al. (2008). Multiple renal cysts, urinary concentration defects, and pulmonary emphysematous changes in mice lacking TAZ. Am. J. Physiol. Renal Physiol. *294*, F542–F553.

McLean, G.W., Carragher, N.O., Avizienyte, E., Evans, J., Brunton, V.G., and Frame, M.C. (2005). The role of focal-adhesion kinase in cancer - a new therapeutic opportunity. Nat. Rev. Cancer *5*, 505–515.

Meng, Z., Moroishi, T., Mottier-Pavie, V., Plouffe, S.W., Hansen, C.G., Hong, A.W., Park, H.W., Mo, J.-S., Lu, W., Lu, S., et al. (2015). MAP4K family kinases act in parallel to MST1/2 to activate LATS1/2 in the Hippo pathway. Nat. Commun. *6*, 8357.

Mitchell, K., Szekeres, C., Milano, V., Svenson, K.B., Nilsen-Hamilton, M., Kreidberg, J.A., and DiPersio, C.M. (2009). Alpha3beta1 integrin in epidermis promotes wound angiogenesis and keratinocyte-to-endothelial-cell crosstalk through the induction of MRP3. J. Cell Sci. *122*, 1778–1787.

Mo, J.-S., Meng, Z., Kim, Y.C., Park, H.W., Hansen, C.G., Kim, S., Lim, D.-S., and Guan, K.-L. (2015). Cellular energy stress induces AMPK-mediated regulation of YAP and the Hippo pathway. Nat. Cell Biol. *17*, 500–510.

Moroishi, T., Park, H.W., Qin, B., Chen, Q., Meng, Z., Plouffe, S.W., Taniguchi, K., Yu, F.-X., Karin, M., Pan, D., and Guan, K.L. (2015). A YAP/TAZ-induced feedback mechanism regulates Hippo pathway homeostasis. Genes Dev. *29*, 1271–1284.

Muzumdar, M.D., Tasic, B., Miyamichi, K., Li, L., and Luo, L. (2007). A global double-fluorescent Cre reporter mouse. Genesis *45*, 593–605.

Oldham, M.C., Langfelder, P., and Horvath, S. (2012). Network methods for describing sample relationships in genomic datasets: application to Huntington's disease. BMC Syst. Biol. *6*, 63.

Parsa, S., Kuremoto, K., Seidel, K., Tabatabai, R., Mackenzie, B., Yamaza, T., Akiyama, K., Branch, J., Koh, C.J., Al Alam, D., et al. (2010). Signaling by FGFR2b controls the regenerative capacity of adult mouse incisors. Development *137*, 3743–3752.

Porazinski, S., Wang, H., Asaoka, Y., Behrndt, M., Miyamoto, T., Morita, H., Hata, S., Sasaki, T., Krens, S.F.G., Osada, Y., et al. (2015). YAP is essential for tissue tension to ensure vertebrate 3D body shape. Nature *521*, 217–221.

Prowse, A.B.J., Chong, F., Gray, P.P., and Munro, T.P. (2011). Stem cell integrins: implications for ex-vivo culture and cellular therapies. Stem Cell Res. (Amst.) *6*, 1–12.

Qi, Q., Li, D.Y., Luo, H.R., Guan, K.-L., and Ye, K. (2015). Netrin-1 exerts oncogenic activities through enhancing Yes-associated protein stability. Proc. Natl. Acad. Sci. USA *112*, 7255–7260.

Raghavan, S., Bauer, C., Mundschau, G., Li, Q., and Fuchs, E. (2000). Conditional ablation of beta1 integrin in skin. Severe defects in epidermal proliferation, basement membrane formation, and hair follicle invagination. J. Cell Biol. *150*, 1149–1160.

Reginensi, A., Scott, R.P., Gregorieff, A., Bagherie-Lachidan, M., Chung, C., Lim, D.-S., Pawson, T., Wrana, J., and McNeill, H. (2013). Yap- and Cdc42-dependent nephrogenesis and morphogenesis during mouse kidney development. PLoS Genet. *9*, e1003380.

Sachs, N., Secades, P., van Hulst, L., Kreft, M., Song, J.-Y., and Sonnenberg, A. (2012). Loss of integrin α3 prevents skin tumor formation by promoting epidermal turnover and depletion of slow-cycling cells. Proc. Natl. Acad. Sci. USA *109*, 21468–21473.

Schlegelmilch, K., Mohseni, M., Kirak, O., Pruszak, J., Rodriguez, J.R., Zhou, D., Kreger, B.T., Vasioukhin, V., Avruch, J., Brummelkamp, T.R., and Camargo, F.D. (2011). Yap1 acts downstream of α-catenin to control epidermal proliferation. Cell *144*, 782–795.

Seguin, L., Desgrosellier, J.S., Weis, S.M., and Cheresh, D.A. (2015). Integrins and cancer: regulators of cancer stemness, metastasis, and drug resistance. Trends Cell Biol. *25*, 234–240.

Seidel, K., Ahn, C.P., Lyons, D., Nee, A., Ting, K., Brownell, I., Cao, T., Carano, R.A.D., Curran, T., Schober, M., et al. (2010). Hedgehog signaling regulates the generation of ameloblast progenitors in the continuously growing mouse incisor. Development *137*, 3753–3761.

Sengupta, S., Peterson, T.R., Laplante, M., Oh, S., and Sabatini, D.M. (2010). mTORC1 controls fasting-induced ketogenesis and its modulation by ageing. Nature *468*, 1100–1104.

Suomalainen, M., and Thesleff, I. (2010). Patterns of Wnt pathway activity in the mouse incisor indicate absence of Wnt/beta-catenin signaling in the epithelial stem cells. Dev. Dyn. *239*, 364–372.

Szymaniak, A.D., Mahoney, J.E., Cardoso, W.V., and Varelas, X. (2015). Crumbs3-Mediated Polarity Directs Airway Epithelial Cell Fate through the Hippo Pathway Effector Yap. Dev. Cell *34*, 283–296.

Tang, Y., Rowe, R.G., Botvinick, E.L., Kurup, A., Putnam, A.J., Seiki, M., Weaver, V.M., Keller, E.T., Goldstein, S., Dai, J., et al. (2013). MT1-MMP-dependent control of skeletal stem cell commitment via a β1-integrin/YAP/TAZ signaling axis. Dev. Cell *25*, 402–416.

Tumaneng, K., Schlegelmilch, K., Russell, R.C., Yimlamai, D., Basnet, H., Mahadevan, N., Fitamant, J., Bardeesy, N., Camargo, F.D., and Guan, K.-L. (2012). YAP mediates crosstalk between the Hippo and PI(3)K–TOR pathways by suppressing PTEN via miR-29. Nat. Cell Biol. *14*, 1322–1329.

Varelas, X., Miller, B.W., Sopko, R., Song, S., Gregorieff, A., Fellouse, F.A., Sakuma, R., Pawson, T., Hunziker, W., McNeill, H., et al. (2010). The Hippo pathway regulates Wnt/β-catenin signaling. Dev. Cell *18*, 579–591.

Wabik, A., and Jones, P.H. (2015). Switching roles: the functional plasticity of adult tissue stem cells. EMBO J. *34*, 1164–1179.

Waikel, R.L., Kawachi, Y., Waikel, P.A., Wang, X.-J., and Roop, D.R. (2001). Deregulated expression of c-Myc depletes epidermal stem cells. Nat. Genet. *28*, 165–168.

Wang, J., Xiao, Y., Hsu, C.-W., Martinez-Traverso, I.M., Zhang, M., Bai, Y., Ishii, M., Maxson, R.E., Olson, E.N., Dickinson, M.E., et al. (2016). Yap and Taz play a crucial role in neural crest-derived craniofacial development. Development *143*, 504–515.

White, A.C., Khuu, J.K., Dang, C.Y., Hu, J., Tran, K.V., Liu, A., Gomez, S., Zhang, Z., Yi, R., Scumpia, P., et al. (2014). Stem cell quiescence acts as a tumour suppressor in squamous tumours. Nat. Cell Biol. *16*, 99–107.

Wu, X., Quondamatteo, F., Lefever, T., Czuchra, A., Meyer, H., Chrostek, A., Paus, R., Langbein, L., and Brakebusch, C. (2006). Cdc42 controls progenitor cell differentiation and beta-catenin turnover in skin. Genes Dev. *20*, 571–585.

Xin, M., Kim, Y., Sutherland, L.B., Qi, X., McAnally, J., Schwartz, R.J., Richardson, J.A., Bassel-Duby, R., and Olson, E.N. (2011). Regulation of insulin-like growth factor signaling by Yap governs cardiomyocyte proliferation and embryonic heart size. Sci. Signal. *4*, ra70.

Xin, M., Kim, Y., Sutherland, L.B., Murakami, M., Qi, X., McAnally, J., Porrello, E.R., Mahmoud, A.I., Tan, W., Shelton, J.M., et al. (2013). Hippo pathway effector Yap promotes cardiac regeneration. Proc. Natl. Acad. Sci. USA *110*, 13839–13844.

Yilmaz, O.H., Valdez, R., Theisen, B.K., Guo, W., Ferguson, D.O., Wu, H., and Morrison, S.J. (2006). Pten dependence distinguishes haematopoietic stem cells from leukaemia-initiating cells. Nature *441*, 475–482.

Yu, F.-X., Zhao, B., Panupinthu, N., Jewell, J.L., Lian, I., Wang, L.H., Zhao, J., Yuan, H., Tumaneng, K., Li, H., et al. (2012). Regulation of the Hippo-YAP pathway by G-protein-coupled receptor signaling. Cell *150*, 780–791.

Yu, F.-X., Zhao, B., and Guan, K.-L. (2015). Hippo Pathway in Organ Size Control, Tissue Homeostasis, and Cancer. Cell *163*, 811–828.

Zhang, H., Wang, Z., and Zhang, Z. (2013). PP1α, PP1β and Wip-1 regulate H4S47 phosphorylation and deposition of histone H3 variant H3.3. Nucleic Acids Res. *41*, 8085–8093.

Zhao, B., Wei, X., Li, W., Udan, R.S., Yang, Q., Kim, J., Xie, J., Ikenoue, T., Yu, J., Li, L., et al. (2007). Inactivation of YAP oncoprotein by the Hippo pathway is involved in cell contact inhibition and tissue growth control. Genes Dev. *21*, 2747–2761.

Zhao, B., Li, L., Tumaneng, K., Wang, C.-Y., and Guan, K.-L. (2010). A coordinated phosphorylation by Lats and CK1 regulates YAP stability through SCF(beta-TRCP). Genes Dev. *24*, 72–85.

Zheng, Y., Wang, W., Liu, B., Deng, H., Uster, E., and Pan, D. (2015). Identification of Happyhour/MAP4K as Alternative Hpo/Mst-like Kinases in the Hippo Kinase Cascade. Dev. Cell *34*, 642–655.

Zhou, D., Zhang, Y., Wu, H., Barry, E., Yin, Y., Lawrence, E., Dawson, D., Willis, J.E., Markowitz, S.D., Camargo, F.D., and Avruch, J. (2011). Mst1 and Mst2 protein kinases restrain intestinal stem cell proliferation and colonic tumorigenesis by inhibition of Yes-associated protein (Yap) overabundance. Proc. Natl. Acad. Sci. USA *108*, E1312–E1320.

STAR★METHODS

KEY RESOURCES TABLE

REAGENT or RESOURCE	SOURCE	IDENTIFIER
Antibodies		
Rabbit monoclonal anti-Non-phospho-4E-BP1 (Thr46) (87D12)	Cell Signaling Technology	Cat# 4923S, RRID:AB_659944
Rabbit polyclonal anti-Ameloblastin	Santa Cruz Biotechnology	Cat# sc-50534, RRID:AB_2226393
Rabbit polyclonal anti-Amelogenin (FL-191)	Santa Cruz Biotechnology	Cat# sc-32892, RRID:AB_2226455
Rat monoclonal anti-BrdU [BU1/75 (ICR1)]	Abcam	Cat# ab6326, RRID:AB_305426
Rabbit polyclonal anti-CDC42 (P1)	Santa Cruz Biotechnology	Cat# sc-87, RRID:AB_631213
Mouse monoclonal anti-CDC42-GTP	NewEast Biosciences	Cat# 26905, RRID:AB_1961759
Mouse monoclonal anti-GAPDH	Acris Antibodies GmbH	Cat# ACR001P, RRID:AB_1616730
Chicken polyclonal anti-GFP	Abcam	Cat# ab13970, RRID:AB_300798
Rabbit polyclonal anti-ITGA3	From: C. Michael DiPersio; Aggarwal et al., 2014	N/A
Rabbit monoclonal anti-Ki67 (SP6)	Thermo Fisher Scientific	Cat# RM-9106-S0, RRID:AB_2341197
Rabbit monoclonal anti-Merlin (D3S3W)	Cell Signaling Technology	Cat# 12888S
Rabbit polyclonal anti-MST1-2/STK3-4	Bethyl	Cat# A300-466A
Goat polyclonal anti-NDR1 (N-14)	Santa Cruz Biotechnology	Cat# sc-46184, RRID:AB_2196799
Rabbit monoclonal anti-Phospho-4E-BP1 (Thr37/46) (236B4)	Cell Signaling Technology	Cat# 2855S, RRID:AB_560835
Rabbit polyclonal anti-PAK1/2/3	Cell Signaling Technology	Cat# 2604, RRID:AB_2160225
Mouse monoclonal anti-P-cadherin (NCC-CAD-299)	Thermo Fisher Scientific	Cat# 13-5800, RRID:AB_2533023
Rabbit polyclonal anti-pFAK (Phospho-Tyr397)	Assay Biotech	Cat# A0925, RRID:AB_10683791
Rabbit polyclonal anti-pLATS1 (Thr1079)	Cell Signaling Technology	Cat# 9157S, RRID:AB_2133515
Rabbit polyclonal anti-pMerlin (Ser518)	Rockland	Cat# 600-401-414, RRID:AB_2149813
Rabbit monoclonal anti-pMerlin (Ser518) (D5A4I)	Cell Signaling Technology	Cat# 13281
Rabbit polyclonal anti-pNDR1/2 (Phospho-Thr444/442)	Biorbyt	Cat# orb335842
Mouse monoclonal anti-PP1 (E-9)	Santa Cruz Biotechnology	Cat# sc-7482, RRID:AB_628177
Goat monoclonal anti-PP2A-Calpha/beta (C-20)	Santa Cruz Biotechnology	Cat# sc-6110, RRID:AB_216962
Rabbit polyclonal anti-pPAK1 (Thr423)/ pPAK2 (Thr402)	Cell Signaling Technology	Cat# 2601S, RRID:AB_330220
Rabbit polyclonal anti-p70 S6 Kinase (Phospho-Thr389)	Assay Biotech	Cat# A0533, RRID:AB_10682683
Rabbit polyclonal anti-phospho-p70 S6 Kinase (Thr389)	Cell Signaling Technology	Cat# 9205, RRID:AB_330944
Rabbit polyclonal anti-pSRC (Tyr418)	Signalway	Cat# 11091
Rabbit polyclonal anti-pYAP (Ser127)	Cell Signaling Technology	Cat# 4911S, RRID:AB_2218913
Rabbit monoclonal anti-pYAP (Ser127) (D9W2I)	Cell Signaling Technology	Cat# 13008
Rabbit monoclonal anti-pYAP (Ser397) (D1E7Y)	Cell Signaling Technology	Cat# 13619
Rabbit polyclonal anti-RHEB	ProSci	Cat# 3501, RRID:AB_736009
Rabbit monoclonal anti- p70 S6 Kinase (49D7)	Cell Signaling Technology	Cat# 2708, RRID:AB_390722

(*Continued on next page*)

Continued

REAGENT or RESOURCE	SOURCE	IDENTIFIER
Rabbit polyclonal anti-SerpinH1	ABclonal	Cat# A-2517
Rabbit polyclonal anti-WWTR1 (TAZ)	Sigma-Aldrich	Cat# HPA007415, RRID:AB_1080602
Rabbit polyclonal anti-YAP	Cell Signaling Technology	Cat# 4912, RRID:AB_2218911
Mouse monoclonal anti-YAP (63.7)	Santa Cruz Biotechnology	Cat# sc-101199, RRID:AB_1131430
Rabbit monoclonal anti-YAP (human) [EP1674Y]	Abcam	Cat# ab52771, RRID:AB_2219141
Goat polyclonal anti-rabbit IgG (H+L), Alexa Fluor 555 conjugated	Thermo Fisher Scientific	Cat# A21428, RRID:AB_10561552
Goat polyclonal anti-rat IgG (H+L), Alexa Fluor 555 conjugated	Thermo Fisher Scientific	Cat# A-21434, RRID:AB_2535855
Goat polyclonal anti-chicken IgY (H+L), Alexa Fluor 488 conjugate	Thermo Fisher Scientific	Cat# A-11039, RRID:AB_2534096
Biotinylated goat polyclonal anti-rabbit IgG	Vector Laboratories	Cat# BA-1000, RRID:AB_2313606
Biotinylated goat polyclonal anti-mouse IgG	Vector Laboratories	Cat# BA-9200, RRID:AB_2336171
Goat polyclonal anti-rabbit IgG, HRP	Cell Signaling Technology	Cat# 7074, RRID:AB_2099233
Horse polyclonal anti-mouse IgG, HRP	Cell Signaling Technology	Cat# 7076, RRID:AB_330924
Mouse monoclonal TrueBlot anti-rabbit IgG, HRP	Rockland	Cat# 18-8816-31, RRID:AB_2610847
Rat monoclonal TrueBlot anti-mouse IgG, HRP	Rockland	Cat# 18-8817-31, RRID:AB_2610850
SmartBlot anti-goat IgG, HRP	Vicgene	Cat# va-6000-001
Chemicals, Peptides, and Recombinant Proteins		
(-)-Blebbistatin	EMD Millipore	Cat# 203391; CAS: 856925-71-8
Erlotinib HCl	Selleck Chemical	Cat# OSI-744; CAS: 183319-69-9
Ki16425	Selleck Chemical	Cat# S1315; CAS: 355025-24-0
Latrunculin A, Latrunculia magnifica	EMD Millipore	Cat# 428021; CAS: 76343-93-6
Okadaic acid, Prorocentrum sp.	EMD Millipore	Cat# 495609; CAS: 78111-17-8
PF-573228	Selleck Chemical	Cat# S2013; CAS: 869288-64-2
PP2	EMD Millipore	Cat# 529573; CAS: 172889-27-9
Rapamycin	Selleck Chemical	Cat# S1039; CAS: 53123-88-9
Recombinant Mouse EGF Protein	R&D Systems	Cat# 2028-EG; Accession# NP_034243
Recombinant Human FGF basic	R&D Systems	Cat# 233-FB; Accession# P09038
Y-27632	Selleck Chemical	Cat# S1049; CAS: 129830-38-2
Critical Commercial Assays		
In Situ Cell Death Detection Kit, TMR red	Sigma-Aldrich	Cat# 12156792910
SuperSignal West Pico Chemiluminescent Substrate	Thermo Fisher Scientific	Cat# 34080
TSA Cyanine 3 Tyramide Reagent Pack	Perkin Elmer	Cat# SAT704B001EA
VECTASTAIN Elite ABC HRP Kit (Peroxidase, Standard)	Vector Laboratories	Cat# PK-6100
Deposited Data		
Raw and normalized microarray data	This paper	GEO: GSE87132
Experimental Models: Organisms/Strains		
Mouse: *CAT-Rho-K DN/3-1*	From: Jeffrey Bush, Kobayashi et al., 2004	RBRC# RBRC01294
Mouse: *Cdc42*^{tm1Brak}	From: Cord Brakebusch; Wu et al., 2006	MGI: 3619134
Mouse: *Col1a1*$^{tm1(tetO-YAP1*)Fcam}$	From: Fernando Camargo; Camargo et al., 2007	MGI: 5316453
Mouse: *Gt(ROSA)26Sor*$^{tm4(ACTB-tdTomato,-EGFP)Luo}$	The Jackson Laboratory; Muzumdar et al., 2007	RRID: IMSR_JAX:007676; Cat# 007676; MGI: 3716464
Mouse: *Itga3*$^{f/f}$	From: Michael DiPersio; Mitchell et al., 2009	N/A

(*Continued on next page*)

Continued

REAGENT or RESOURCE	SOURCE	IDENTIFIER
Mouse: *Lats1*$^{tm1.1Jfm}$	From: Randy Johnson; Heallen et al., 2011	RRID: IMSR_JAX:024941; MGI: 5568586
Mouse: *Lats2*$^{tm1.1Jfm}$	From: Randy Johnson; Heallen et al., 2011	RRID: IMSR_JAX:025428; MGI: 5568589
Mouse: *Ptk2*^{tm1Lfr}	From: Valerie Weaver; Beggs et al., 2003	MGI:2684666
Mouse: *Rac1*^{tm1Djk}	From: Jeffrey Bush; Glogauer et al., 2003	RRID: IMSR_JAX:005550; MGI: 2663662
Mouse: *Rptor*$^{tm1.1Dmsa}$	From: Ajay Chawla; Sengupta et al., 2010	RRID: IMSR_JAX:013188; MGI: 4879103
Mouse: *RhoA*$^{f/f}$	From: Cord Brakebusch; Jackson et al., 2011	N/A
Mouse: *Stk3*$^{tm1.1Rjo}$	From: Randy Johnson; Lu et al., 2010	MGI: 4430537
Mouse: *Stk4*$^{tm1.1Rjo}$	From: Randy Johnson; Lu et al., 2010	RRID: IMSR_JAX:017635; MGI: 4430536
Mouse: *Tg(KRT14-cre)1Amc*	Dassule et al., 2000	RRID: IMSR_JAX:004782; MGI: 2445832
Mouse: *Tg(KRT14-cre/ERT2)1Ipc*	Li et al., 2000	MGI: 2177426
Mouse: *Wwtr1*$^{tm1.1Eno}$	From: Randy Johnson; Xin et al., 2011	MGI: 5544289
Mouse: *Yap1*$^{tm1.1Eno}$	From: Randy Johnson; Xin et al., 2011	MGI: 5446483
Recombinant DNA		
pcDNA Flag Yap1	Addgene	Cat# 18881
pCMV-flag S127A YAP	Addgene	Cat# 27370
pCMV-Flag YAP S381A	Addgene	Cat# 27377
pQCXIH-Flag-YAP-S127/381A	Addgene	Cat# 33069
Sequence-Based Reagents		
Primer sequences	See Table S2	N/A
Taz RNA probe	This paper	N/A
Yap RNA probe	This paper	N/A
Software and Algorithms		
ImageJ	https://imagej.nih.gov/ij/	N/A
ImageJ Colocalization plugin	https://imagej.nih.gov/ij/plugins/colocalization.html	N/A
SampleNetwork R function	Oldham et al., 2012	N/A
ComBat R function	Johnson et al., 2007	N/A

CONTACT FOR REAGENT AND RESOURCE SHARING

Further information and requests for reagents may be directed to, and will be fulfilled by, the Lead Contact, ophir.klein@ucsf.edu

EXPERIMENTAL MODEL AND SUBJECT DETAILS

Mouse lines and induction of alleles

K14^{CreER} (Li et al., 2000), *K14*^{Cre} (Dassule et al., 2000), *YAP*^{S127A} (Camargo et al., 2007), *R26*$^{mT/mG}$ (Muzumdar et al., 2007), and conditional alleles of *Cdc42* (Wu et al., 2006), *Fak* (Beggs et al., 2003), *Itga3* (Mitchell et al., 2009), *Rac1* (Glogauer et al., 2003), *RhoA* (Jackson et al., 2011), dominant negative *Rock2* (Kobayashi et al., 2004), *Rptor* (Sengupta et al., 2010), *Lats1* and *Lats2* (Heallen et al., 2011), *Mst1* and *Mst2* (Lu et al., 2010), *Yap* (Xin et al., 2011) and *Taz* (*Wwtr1*) (Xin et al., 2013) were group housed and genotyped as previously published (sequences provided in Table S3). The strains of these mice were the same as previously described in their respective references at the time of acquisition but were subsequently maintained on mixed backgrounds after breeding between different lines. All conditional lines were crossed to *K14*^{CreER}, except *Itga3*$^{f/f}$, which was bred to *K14*^{Cre}. Adult mutant and Cre-negative littermate control mice, both males and females, at 8 weeks of age were selected randomly and used in all experiments. No criteria were employed to exclude the use of any mouse for experiments. For CreER activation, 5 mg of tamoxifen dissolved in corn oil was delivered to both mutant and control mice through intraperitoneal injection. All experiments involving mice were approved by the Institutional Animal Care and Use Committee of the University of California, San Francisco (protocol #AN151723).

Sample sources for laCL cells and explants

For colony formation assays, dissected laCLs from *K14^{CreER};R26$^{mT/mG}$* and *Yap/Taz^{cKO};R26$^{mT/mG}$* mice 48 hr after tamoxifen injection were used to generate dissociated cells. For explant culture studies, dissected proximal incisors from wild-type C57BL/6 mice were used, either in conjunction with chemical inhibitors or for electroporation.

METHOD DETAILS

Tissue preparation and histological analysis

Euthanized mice were first perfused using PBS and then 4% paraformaldehyde (PFA) in PBS. Mouse mandibles were dissected away from the rest of the cranium and fixed with 4% PFA in PBS overnight at 4°C. Mandibles were subsequently washed with PBS, dehydrated in 70% ethanol in water through serial ethanol washes, and equilibrated to paraffin using Leica ASP300S. Mandibles were then embedded in paraffin and sectioned at 6 μm. Hematoxylin & Eosin (H&E) staining was carried out using standard protocols.

Immunofluorescence staining

For immunofluorescence, paraffin sections were rehydrated, and antigen retrieval was performed by sub-boiling slides in pH 6.2 citrate buffer containing 10mM citric acid, 2mM EDTA, 0.05% Tween 20 using microwave for 15 min. For YAP immunostaining, samples were additionally washed with 2N HCl for 5 min. Primary and secondary antibodies used and corresponding dilutions were summarized in Table S4. Samples were blocked in 1X animal-free blocker (Vector Laboratories), supplemented with 2.5% heat inactivated goat serum, 0.02% SDS and 0.1% Triton-X. All antibodies were diluted in the same block without serum. For detection of CDC42-GTP, ITGA3 (Aggarwal et al., 2014), PCAD, p4EBP, pFAK, pMerlin, pS6K1, pSRC, pYAP, RHEB, SerpinH1, TAZ, and YAP, primary antibodies were first detected by biotinylated secondary antibodies (Table S4), and then sequentially amplified using VECTASTAIN Elite ABC HRP Kit (Vector Laboratories) and Tyramide Signal Amplification (PerkinElmer). DAPI (Invitrogen) was used for nuclear staining and all images were acquired using a Leica-TCS SP5 confocal microscope. TUNEL staining was performed according to manufacturer's instructions (Sigma-Aldrich).

In situ hybridization

Section in situ hybridization was performed as previously described (Seidel et al., 2010) on tissue sections using digoxigenin (DIG)-labeled *Yap*, *Taz*, *Amelx*, and *Ambn* probes. *Yap*, *Taz*, *Amelx*, and *Ambn* fragments were subcloned using primers with T7 and T3 binding site-overhangs: *Yap* Fwd 5′-ATATTAATACGACTCACTATAGGGTCAATGCCGTCATGAACCCCAAG-3′, *Yap* Rev 5′-ATATAATTAACCCTCACTAAAGGGCCAGCCAGGATGTGGTCTTGTTC-3′, *Taz* Fwd 5′-ATATTAATACGACTCACTATAGGG CAAGTCGTGGCCACTAGCCTG-3′, *Taz* Rev 5′-ATATAATTAACCCTCACTAAAGGGTCCCGAGGTCAACATTTGTTCCTG-3′, *Amelx* Fwd 5′-ATATTAATACGACTCACTATAGGGCAGCCGTATCCTTCCTAT-3′, *Amelx* Rev 5′-ATATAATTAACCCTCACTAAAGATGCC CTGGTACCACTTCAT-3′, *Ambn* Fwd 5′-ATATTAATACGACTCACTATAGCACTCAGCAGCCACTGCTAC-3′, *Ambn* Rev 5′-ATATA ATTAACCCTCACTAAAGCAGGGTTTTCCACCAATCAC-3′ from a mouse cDNA library that was reverse transcribed using RNA extracted from an E12.5 mouse brain or adult proximal incisors. For probe synthesis, PCR products were directly used in combination with T3 RNA polymerase (Promega) and generated probes were purified using QIAGEN RNeasy. Sections were hybridized with probes at 70°C overnight and then washed in SSC solutions. Bound probes were detected with an alkaline phosphatase conjugated anti-DIG antibody (Roche), followed by colorimetric development using BM Purple (Roche). Bright field images were obtained using a Leica DFC 500 camera with a Leica DM 5000B microscope. For double fluorescent in situ hybridization and immunostaining, a POD-conjugated anti-DIG antibody (Roche) was used, followed by signal detection using Tyramide Signal Amplification (PerkinElmer). Immunostaining for membrane GFP was then performed as described above. Fluorescent images were obtained using a Leica-TCS SP5 confocal microscope.

Microtomography

Mandibles were harvested and dehydrated through ethanol series to 70% ethanol in water. Samples were then soaked in phosphotungstic acid overnight to differentially stain soft tissues for μCT visualization using MicroXCT-200 (Xradia) with a spatial resolution of 0.5 μm. Images acquired were analyzed using Avizo (VSG).

Isolation of laCLs

laCLs were isolated from incisors as previously described (Biehs et al., 2013). In brief, proximal incisors (roughly 2 mm in length) were first collected by removing the surrounding jaw bones and being severed away with a pair of scissors. The dissected proximal incisors were then incubated in 0.8% EDTA in Ca^{2+}/Mg^{2+} free PBS supplemented with 30 μg/ml DNase at 37°C for 30 min to separate the dental epithelium from the mesenchyme and periodontal tissues. laCLs that included both the bulbous portion, as well as the lateral wing-shaped epithelium, were subsequently dissected from the rest of the epithelium and collected in cold PBS for downstream applications.

Explant culture

Dissected proximal incisors were cultured on a 0.4 μm Millicell filter (Millipore) that was rested on a metal mesh (914 μm mesh opening, Spectrum Labs), such that the explants were grown at the liquid-air interface (refer to Figure 3M). The culture media used was

composed of BGJB media (Thermo), 15% fetal calf serum, 200 μg/ml glutamine, 250 μg/ml ascorbic acid, 1% pen/strep, and with chemical inhibitors or DMSO control vehicle. Drugs used include Blebbistatin, Erlotinib, Ki16425, Latrunculin A, okadaic acid, PF573228, PP2, Rapamycin, and Y27632. These chemicals and their concentrations are listed in Table S2. In most cases, explants were cultured for 24 hr at 37°C before collection. Okadaic acid-treated explants were cultured for 12 hr and electroporated incisors were cultured for 8 hr.

Electroporation

Proximal incisors were first isolated as described above and incubated in 0.8% EDTA at 37°C for 10 min to separate the follicle layer from the dental epithelium. 2 μg/μl of DNA in PBS, intermixed with 0.66% carboxymethylcellulose, 1mM $MgCL_2$, and 0.66% fast green, were mouth-pipetted into the space between the follicle layer and the outer enamel epithelium. 3 20 ms long 70V pulses were then applied using custom made platinum electrodes and a BTX-Harvard Apparatus ECM 830 electroporator to induce DNA uptake by OEE cells (Figure 6F). The electroporated samples were then cultured as explants for 8 hr. The following constructs were used for electroporation: pcDNA-Flag-Yap1 (a gift from Yosef Shaul, Addgene plasmid # 18881) (Levy et al., 2008), pCMV-flag-S127A-YAP, pCMV-Flag-YAP-S381A, and pQCXIH-Flag-YAP-S127/381A (gifts from Kunliang Guan, Addgene plasmid # 27370, 27377, and 33069) (Zhao et al., 2007, 2010).

Colony formation assay

To generate single laCL cell suspension, isolated laCLs were incubated with Accumax (Sigma) at 37°C for 30 min, spun down, and dissociated in 10 μl of media (DMEM/F12 (GIBCO), 20 ng/ml EGF (R&D), 25 ng/ml bFGF (R&D), 1X B27 (GIBCO), and 1% pen/strep). The cell suspension was passed through a 40 μm cell strainer (Fisher Scientific) and mixed with 80 μl of cold growth factor-reduced Matrigel (Corning), which was then sandwiched between an activated 18 mm circular cover glass (as prepared in Damljanović et al., 2005) and a Rain-X treated cover glass. Once the Matrigel was set, the Rain-X treated cover glass was removed and cells were cultured in media at 37°C for 72 hr before counting colonies.

Western blot and immunoprecipitation

Western blot and immunoprecipitation were performed based on manufacturer's instructions (Thermo Fisher Scientific). For western blot, Isolated laCLs were pooled and lysed using RIPA buffer (Thermo Fisher Scientific) supplemented with 1X Halt Protease and Phosphatase Inhibitor (Thermo Fisher Scientific) and 0.2 mM PMSF for 30 min at 4°C. Protein extracts were loaded in 4%–12% Bis-Tris gel (Thermo Fisher Scientific), transferred to nitrocellulose membrane, blocked with SuperBlock T20 (TBS) (Thermo Fisher Scientific), and immunobloted with primary antibodies (Table S4) at 4°C overnight. After incubation with appropriate HRP-conjugated secondary antibodies (Table S4) in room temperature for 1 hr, signals were detected with SuperSignal West Pico Chemiluminescent Substrate (Thermo Fisher Scientific) and images were taken using Image Quant LAS 4000. For immunoprecipitation, laCLs were lysed using IP Lysis Buffer (Thermo Fisher Scientific) for 2 hr at 4°C. Lysates were incubated with antibodies against YAP (Santa Cruz) or CDC42-GTP (NewEast) that have been crosslinked with anti-mouse IgG Dynabeads (Thermo Fisher Scientific) for 2 hr at 4°C. Bound proteins were eluted in LDS Sample Buffer (Thermo Fisher Scientific) by heating at 90°C for 10 min and elutes were analyzed by western blot as described above. Quantification was performed using ImageJ (see below). AMELX, AMBN, and RHEB were normalized to GAPDH, p4EBP, pLATS1, pNDR1/2, pPAK, pS6K1, pYAP-S127, and pYAP-S397 were normalized to their respective total protein levels, and immunoprecipitated active CDC42 and PP1A were normalized to total CDC42 input and total YAP pulled-down respectively.

Expression profiling by microarray

Expression profiling of control and *Yap/Taz*^{cKO} laCLs by microarray was done in triplicates and the RNA used for each sample was extracted from 8 laCLs (2 males and 2 females) using the QIAGEN RNeasy micro kit. Total RNA quality was assessed using a Pico Chip on an Agilent 2100 Bioanalyzer (Agilent Technologies, Palo Alto, CA). Microarray was performed on Illumina Mouse Ref 8 v2.0 chips at the UCLA Neuroscience Genomics Core (UNGC). Raw bead-level microarray data were minimally processed by the UNGC (no normalization or background correction) using BeadStudio software (Illumina, San Diego, CA). Preprocessing of data was performed within the R statistical computing environment (R; http://cran.us.r-project.org). The SampleNetwork R function (Oldham et al., 2012) was used to determine outlying samples, assess technical batch effects, and perform data normalization. No outlying samples were removed. However, after quantile normalization a technical batch effect was found to be associated with "ArrayID" and was corrected using the ComBat R function (Johnson et al., 2007) with the type of sample (control or *Yap/Taz*^{cKO}) as a covariate. Following data preprocessing, differential expression analysis was performed to identify genes that were significantly up- or down-regulated in *Yap/Taz*^{cKO} laCLs (n = 4) relative to controls (n = 3). Probes on the microarray that were detected above background levels in more than one sample (n = 17174) were included in the analysis. Differential expression analysis was performed on log2-transformed expression data using the bayesT function from the Cyber-T R package (Baldi and Long, 2001; Kayala and Baldi, 2012). The p values were adjusted to account for multiple testing using the false discovery rate (FDR) approach (Benjamini and Hochberg, 1995), and probes with FDR $p < 0.05$ were considered to be differentially expressed. However, as we took consideration that Cre recombination in *Yap/Taz*^{cKO} was not 100%, we also verified expression of genes that were above FDR $p > 0.05$ using immunostaining or qPCR. Gene enrichment analysis was performed using Gene Set Enrichment Analysis (GSEA) (http://software.broadinstitute.org/gsea/index.jsp).

qPCR analysis

For qPCR analysis, RNA from isolated Cre negative control and *Yap/Taz*^{cKO} laCLs was reverse-transcribed to cDNA using SensiFAST cDNA Synthesis Kit (Bioline). qPCR was performed using iTAQ CYBR green (Biorad) and the Eppendorf Realplex^2 with the following conditions: 3 min at 95°C and 40 cycles of amplification (15 s at 95°C and 30 s at 60°C). The primer sets used are listed in Table S3. All measurements were normalized to *Ppia* (peptidylprolyl isomerase A) and the relative changes between control and *Yap/Taz*^{cKO} laCLs were determined using the $2^{-\Delta\Delta CT}$ *method* (Livak and Schmittgen, 2001).

STATISTICAL ANALYSIS

Statistics

All bar graphs display mean ± SD (standard deviation) with the exception of the qPCR result, which is shown as mean ± SEM (standard error of mean). Numbers of animals used for each experiment are detailed in Table S5. p values were derived from unpaired two tailed Student's t tests, assuming unequal variance (*$p < 0.05$; **$p < 0.01$; ***$p < 0.001$).

ImageJ image analysis

Colocalization of YAP or TAZ with DAPI was measured using the ImageJ plugin "Colocalization" (contributed by Pierre Bourdoncle). For determining percentage of immunostained area, positive immunofluorescence signals in TA or SR regions were first converted to 8 bit binary images and measured using the "Analyze Particles" function. The derived area was then divided by the total area of TA or SR regions to calculate the percentage of positive immunostaining. To determine average immunostaining pixel intensity, total pixel intensity in TA or SR regions was measured using the ImageJ "Measure" function and then divided by the total area of TA or SR regions. To compare average pixel intensity of immunostaining between Cre-recombined (GFP-positive) and non-recombined (GFP-negative) cells in mutant laCLs, membrane GFP signal was adjusted for thresholds and converted to a mask with holes filled. Immunostaining pixel intensity was then measured within and outside the masked regions, and divided by the total area of the masked and unmasked space respectively. When calculating nuclear YAP pixel intensity, an additional mask was created using DAPI signals. For western blot quantification, we used the inbuilt function for "Gels" to first convert band intensities into histograms, from which the area under the curve can be measured using the Wand tool and the relative expression between control and mutant samples were calculated.

DATA AVAILABILITY

The accession number for the microarray data reported in this paper is GEO: GSE87132.